NAVAL POSTGRADUATE SCHOOL

MONTEREY, CALIFORNIA

THESIS

WAVE REFRACTION OVER COMPLEX NEARSHORE BATHYMETRY

by

Scott Douglas Peak

December 2004

Thesis Advisor: Thomas H.C. Herbers
Second Reader: Edward B. Thornton

Approved for public release; distribution unlimited

THIS PAGE INTENTIONALLY LEFT BLANK

REPORT DOCUMENTATION PAGE			Form Approved OMB No. 0704-0188
Public reporting burden for this collection of information is estimated to average 1 hour per response, including the time for reviewing instruction, searching existing data sources, gathering and maintaining the data needed, and completing and reviewing the collection of information. Send comments regarding this burden estimate or any other aspect of this collection of information, including suggestions for reducing this burden, to Washington headquarters Services, Directorate for Information Operations and Reports, 1215 Jefferson Davis Highway, Suite 1204, Arlington, VA 22202-4302, and to the Office of Management and Budget, Paperwork Reduction Project (0704-0188) Washington DC 20503.			
1. AGENCY USE ONLY *(Leave blank)*	**2. REPORT DATE** December 2004	**3. REPORT TYPE AND DATES COVERED** Master's Thesis	
4. TITLE AND SUBTITLE: Wave Refraction Over Complex Nearshore Bathymetry			**5. FUNDING NUMBERS**
6. AUTHOR(S) Scott Douglas Peak			
7. PERFORMING ORGANIZATION NAME(S) AND ADDRESS(ES) Naval Postgraduate School Monterey, CA 93943-5000			**8. PERFORMING ORGANIZATION REPORT NUMBER**
9. SPONSORING /MONITORING AGENCY NAME(S) AND ADDRESS(ES) N/A			**10. SPONSORING/MONITORING AGENCY REPORT NUMBER**
11. SUPPLEMENTARY NOTES The views expressed in this thesis are those of the author and do not reflect the official policy or position of the Department of Defense or the U.S. Government.			
12a. DISTRIBUTION / AVAILABILITY STATEMENT Approved for public release; distribution unlimited.			**12b. DISTRIBUTION CODE**

13. ABSTRACT (maximum 200 words)

Accurate predictions of nearshore wave conditions are critical to the success of military operations in the littoral environment. Although linear spectral-refraction theory is used by the main operational forecasting centers in the world for these predictions, owing to a lack of field studies its accuracy in regions of complex bathymetry such as steep shoals and submarine canyons is unknown. This study examines the accuracy of linear spectral-refraction theory in areas of complex nearshore bathymetry with three months of extensive wave data collected during the Nearshore Canyon Experiment (NCEX) held in the fall of 2003. The field site, off La Jolla California, is characterized by two submarine canyons that strongly affect the propagation of long period Pacific swell. Data from 7 directional waverider buoys, 17 bottom pressure recorders, and 12 pressure-velocity sensors, were examined and compared to predictions made by a high resolution spectral-refraction model. Analysis reveals large spatial variation in wave heights over the area especially in the vicinity of the canyon heads, where wave heights vary by as much as an order of magnitude over a few hundred meters. This extreme variation in wave conditions across the canyons is surprisingly well described by refraction theory with typical errors of nearshore wave height predictions of about 20 percent.

14. SUBJECT TERMS Refraction, Swell Transformation, Scripps Canyon, NCEX, Nearshore Wave Model			**15. NUMBER OF PAGES** 93
			16. PRICE CODE
17. SECURITY CLASSIFICATION OF REPORT Unclassified	**18. SECURITY CLASSIFICATION OF THIS PAGE** Unclassified	**19. SECURITY CLASSIFICATION OF ABSTRACT** Unclassified	**20. LIMITATION OF ABSTRACT** UL

NSN 7540-01-280-5500 Standard Form 298 (Rev. 2-89)
Prescribed by ANSI Std. 239-18

THIS PAGE INTENTIONALLY LEFT BLANK

Approved for public release; distribution unlimited.

WAVE REFRACTION OVER COMPLEX NEARSHORE BATHYMETRY

Scott Douglas Peak
Lieutenant, Royal Australian Navy
B.Sc., University of New South Wales, 1994
Grad. Dip. Met., Bureau Meteorology, 1998

Submitted in partial fulfillment of the
requirements for the degree of

MASTER OF SCIENCE IN PHYSICAL OCEANOGRAPHY

from the

NAVAL POSTGRADUATE SCHOOL
December 2004

Author: Scott Douglas Peak

Approved by: Thomas H. C. Herbers
Thesis Advisor

Edward B. Thornton
Second Reader

Mary L. Batteen
Chairman, Department of Oceanography

THIS PAGE INTENTIONALLY LEFT BLANK

ABSTRACT

Accurate predictions of nearshore wave conditions are critical to the success of military operations in the littoral environment. Although linear spectral-refraction theory is used by the main operational forecasting centers in the world for these predictions, owing to a lack of field studies its accuracy in regions of complex bathymetry such as steep shoals and submarine canyons is unknown. This study examines the accuracy of linear spectral-refraction theory in areas of complex nearshore bathymetry with three months of extensive wave data collected during the Nearshore Canyon Experiment (NCEX) held in the fall of 2003. The field site, off La Jolla California, is characterized by two submarine canyons that strongly affect the propagation of long period Pacific swell. Data from 7 directional waverider buoys, 17 bottom pressure recorders, and 12 pressure-velocity sensors, were examined and compared to predictions made by a high resolution spectral-refraction model. Analysis reveals large spatial variation in wave heights over the area especially in the vicinity of the canyon heads, where wave heights vary by as much as an order of magnitude over a few hundred meters. This extreme variation in wave conditions across the canyons is surprisingly well described by refraction theory with typical errors of nearshore wave height predictions of about 20 percent.

THIS PAGE INTENTIONALLY LEFT BLANK

TABLE OF CONTENTS

LIST OF FIGURES

THIS PAGE INTENTIONALLY LEFT BLANK

LIST OF TABLES

THIS PAGE INTENTIONALLY LEFT BLANK

ACKNOWLEDGMENTS

My most heartfelt gratitude goes to my supervisor, Professor Tom Herbers. This thesis is a testament to his enthusiastic, kind and expert teaching. His encouragement to travel throughout the USA and understanding that surfing and golf are high priority activities, were also always appreciated. I would also like to thank Paul Jessen for all his help during this study, particularly with the large amount of data processing involved in this study. Without his knowledge and patient explanations of MATLAB programming, this study would not have been completed. Thanks also goes to Dr. Bill O'Reilly for providing me with the working spectral-refraction model and CDIP buoy data. His work in setting up the model for the NCEX region meant that making model predictions was a smooth process. Much appreciation also goes to Mark Orzech for providing me with the ray plotting programs and bathymetry data sets. I also thank Professor Ed Thornton for agreeing to be my second reader and for giving me the opportunity to study the waves at Black's Beach first-hand, from my surfboard during NCEX. Lastly I would like to thank all my new American friends, particularly my American sponsors Billy and Diana Roeting, for making the last 18 months a very enjoyable, exciting and rewarding time. I hope to be able to return your kindness when you all come and visit me 'downunder' in Australia one day.

THIS PAGE INTENTIONALLY LEFT BLANK

I. INTRODUCTION

A. MOTIVATION AND OBJECTIVE

Waves are among the most impressive phenomena in the ocean, at times displaying the most powerful forces in nature, overwhelming ships and structures at sea and devastating coastlines and coastal structures. Although there are many different types of ocean waves, wind-generated surface gravity waves have received the most attention because of their impact on the coastal environment. Recreational boating and surfing, commercial fishing and shipping, and coastal zone development are only cursory examples of activities that are affected by ocean surface waves. For military operations, knowledge of the coastal wave climate is critical to the success or failure of amphibious landings, mine warfare, special forces insertions and other operations in the nearshore environment.

The extent to which waves influence so many processes and operations in the marine environment, has driven a need for accurate wave prediction models. Today the main operational forecasting centers in the world use global wave models such as the Wave-Model (WAM) (Komen et al. 1994) and WavewatchIII (Tolman 1998), to forecast the generation of waves and their propagation throughout the deep ocean basins. The operational parameters of these models are largely constrained by computational demands, with typical global resolution of 1-degree latitude and longitude to a fraction of a degree in regional applications. While well suited for large-scale wave propagation, this resolution is too coarse to adequately handle bathymetry effects such as refraction in coastal areas. Hence bathymetry resolving shallow water wave models such as Simulating Waves Nearshore (SWAN) (Booij et al. 1999) and Refraction-Diffraction (REFDIF) (Kirby and Dalrymple 1994), have been developed to handle wave forecasts in smaller coastal regions (typically with dimensions ten to a few hundred kilometers). Although REFDIF also includes diffraction, the central process described in both models is refraction by depth variations. However refraction theory is formally valid only in areas of slowly varying depth and its accuracy in regions with abrupt bathymetry such as steep shoals or submarine canyons is unknown. Few field studies have been conducted to test the limits of the refraction approximation over complex bathymetry. This study

aims to investigate the accuracy of refraction theory in areas of abrupt nearshore bathymetry using data collected during the Nearshore Canyon Experiment (NCEX) held in the fall of 2003 off La Jolla, California. Data from an extensive array of instruments deployed for 3 months in the vicinity of Scripps and La Jolla submarine canyons were examined and compared to refraction predictions.

B. BACKGROUND

The transfer of energy from the wind to the sea surface generates surface gravity waves. Their development depends primarily on three factors, the strength of the wind, the duration that the wind blows for, and the length of open water over which it blows (or fetch). As waves travel away from the area where they were generated they disperse into groups of similar heights and periods, called 'swell waves'. Swell waves are able to travel, virtually unchanged for thousands of miles and have been tracked across ocean basins (Snodgrass et al 1966). However, as swells propagate into shallow coastal areas, they become increasingly influenced by interactions with the underlying sea floor. In regions of complex bathymetry, the wave properties may be transformed in such a way to produce large variations in wave energy and directions along the coast causing a focusing of wave energy on shoals and headlands. This transformation is generally the result of a number of processes including refraction, diffraction and reflection. While diffraction and reflection are complex processes that tend to disperse energy laterally away from sharp bathymetric features, the dominant process is often refraction (Munk and Traylor 1947).

1. Wave Transformation by Refraction

Wave refraction results from the dependence of wave phase velocity upon depth. As waves enter shallow water, the lower depth and consequent slower rate of advance causes the wave front to bend (or refract) towards shallower areas. Monochromatic wave trains approaching at an angle to a beach with straight and parallel contours are progressively rotated to become more parallel to the shoreline. This phenomenon is analogous to the bending of light rays as they pass through media of differing refractive indices, described by Snell's law of geometrical optics. For waves propagating over uneven two-dimensional bathymetry, refraction can cause either a divergence or convergence of wave energy and associated changes in wave height. A convenient

method to represent this is the use of wave rays. A ray is always locally orthogonal to the wave crests and indicates the direction of wave propagation. Linear refraction theory assumes conservation of wave energy flux between two rays, and thus regions of converging (diverging) rays correspond to higher (lower) wave conditions (U.S. Army CERC 2001). In regions of varying bathymetry, the transformation of wave height and direction from deep to shallow water can be found graphically by plotting ray trajectories to form a refraction diagram. Such analysis typically shows that rays converge on shallow regions associated with headlands, shoals and submarine ridges. In contrast, rays diverge from the deeper waters associated with bays and submarine canyons. Examples are given in Kinsman (1965), Komar (1998), and U.S Army CERC (2001).

In a pioneering study of the refraction of ocean waves, Munk and Traylor (1947) constructed ray diagrams to study the effect of bottom topography on wave transformation over two submarine canyons offshore of La Jolla near San Diego. La Jolla Canyon and its tributary, Scripps Canyon, are unusually steep canyons that extend to within 300 meters of the shoreline. The NCEX experiment was conducted at this very same site, and hence a detailed description of the bottom topography and offshore wave climate of this area is presented in Chapter II. For typical swell conditions in this region, Munk and Traylor (1947) compared theoretical wave refraction estimates with visual observations of wave height made by Naval officers stationed along the adjacent shoreline (Figure 1). Figure 1 illustrates the apparent transformation of 14-second swell propagating over the canyons from the WNW. Prominent features are the region of convergence between stations I and J, resulting in large waves north of Scripps Canyon and in contrast, areas of divergence causing relatively lower wave heights between stations I and C. Considering the imprecision of visual observations and difficulty in producing accurate refraction diagrams, the agreement between predicted and observed wave heights was quite good.

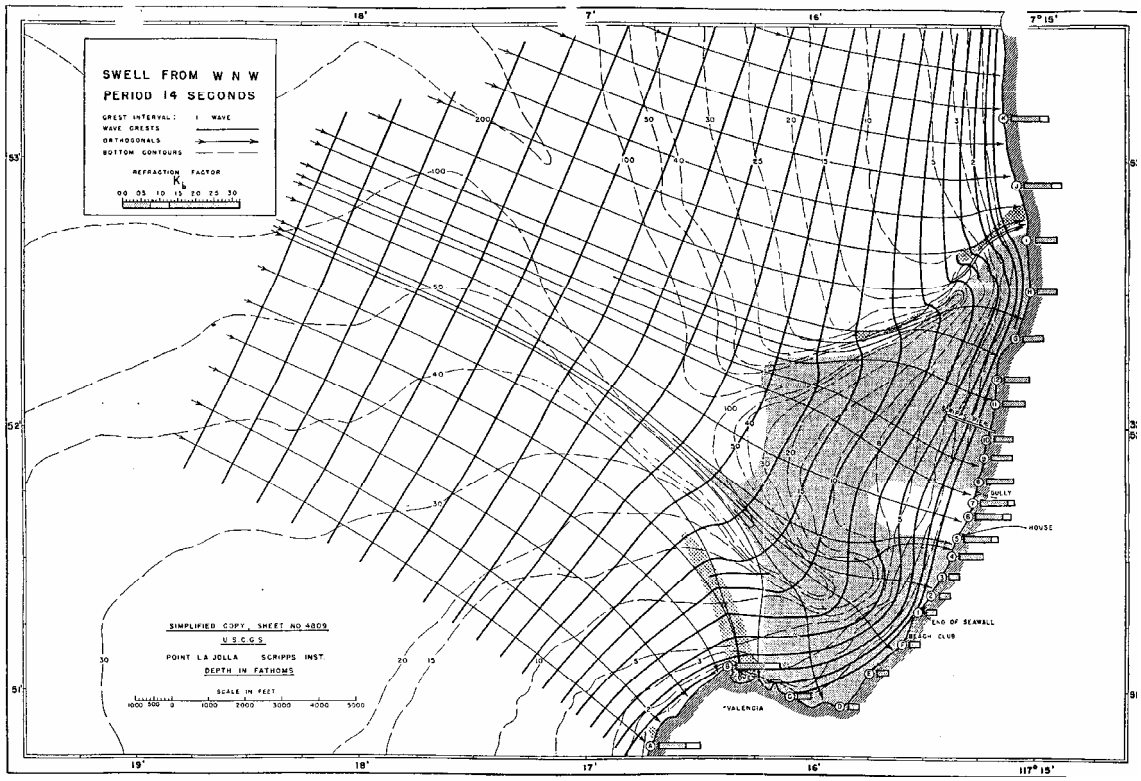

Figure 1. Refraction diagram for 14 second waves from the WNW showing wave crests and rays. The dashed lines represent bottom contours in fathoms (Scripps Canyon to the north), the shore-parallel dark solid lines are wave crests, and the shore-normal light solid lines with arrows are ray trajectories. The length of the boxes adjacent to each station is proportional to wave height. (From: Munk and Traylor 1947)

Whereas Munk and Traylor (1947) plotted successive wave crests to infer wave rays, Munk and Arthur (1952), developed a more advanced technique for the construction of ray trajectories through the use of a set of ray equations, reviewed in Chapter V. Shallow water wave height and direction can be predicted by refracting monochromatic wave trains from deep to shallow water, a technique named *forward ray tracing* (O'Reilly and Guza, 1991). Pierson et al. (1955) used this method to construct refraction diagrams over the Hudson submarine canyon on the outer shelf of New York Harbor. The forward ray tracing technique for monochromatic wave trains breaks down at caustics, where two rays with the same frequency and deep water angle cross. At the caustic, the predicted wave energy becomes infinite and hence this method of analysis is invalid (Kinsman (1965). Longuet-Higgins (1957) showed that this singularity does not

occur for a continuous spectrum of waves, and derived a theory for wave spectra transformation by refraction based on the conservation of the energy spectral density in the wavenumber domain along a wave ray. Practically, the shallow water spectrum is obtained by *back-refracting* rays for all possible frequencies and directions from a specific location to deep water and applying the Longuet-Higgins (1957) conservation law to the corresponding deep water spectrum. Models based on this *backward ray tracing* technique are more robust than models based on forward ray tracing, particularly when handling caustics (O'Reilly and Guza 1991). Although rays still cross, the energy predicted remains finite everywhere because the caustics for a finite bandwidth are spatially distributed over a finite region. O'Reilly and Guza (1991) showed that accurate predictions can be obtained with spectral-refraction models, even over complicated bathymetry with severe caustics.

2. Wave Transformation by Combined Refraction and Diffraction

Refraction theory assumes that for steady state conditions, the energy flux between wave rays is conserved. When waves propagate through regions of abrupt depth variations causing extreme convergence or divergence of wave rays, this assumption may not hold. Instead, the process of diffraction bends the wave crests, transferring energy away from the caustic regions. This phenomenon is most noticeable when waves encounter a surface-piercing obstacle, such as a breakwater or an island. After passing the obstacle, waves turn and carry energy into the sheltered region behind the obstacle.

Recent advances in computing power have seen considerable development in wave transformation models that include the combined effect of refraction and diffraction (Komar 1998). Berkoff (1972) first derived a so-called 'mild-slope' equation valid for small bottom slopes (Massel 1996). This type of model was restricted to the prediction of wave transformation in small areas of harbors and around structures. Radder (1979) applied the parabolic equation method (PEM) to the mild-slope equation, permitting its application to larger coastal areas, although the PEM approximation is restricted to waves propagating at small angles relative to the principle wave direction. Kirby (1986) subsequently introduced higher-order PEM methods that allow for slightly larger angles of propagation. O'Reilly and Guza (1991) successfully applied Kirby's model to coastal areas off Southern California.

Refraction-diffraction models based on the mild-slope equation have been shown to yield satisfactory results for mean bottom slopes up to 1:3 (Booij 1983). However, restrictive assumptions concerning the vertical structure of the wave field render them inappropriate in areas of steep bottom slopes (Athanassoulis and Belibassakis 1999). Recent research has concentrated on improving the mild-slope equation models in areas of steep bathymetry, but the application of these 'extended mild-slope' equation models (Massel 1993, Porter and Staziker 1995), to large coastal areas is still prohibitively expensive.

Even with the intense development of combined refraction-diffraction models, the magnitude of diffraction in areas of actual complex bathymetry remains unknown. The most widely used parabolic approximations to the mild-slope equations may be inaccurate in areas where refraction causes large changes in wave direction (Herbers et al. 2000). In addition, high-resolution predictions for large coastal areas (in the order of tens of kilometers), are computationally demanding. O'Reilly and Guza (1993) pointed out the need for a supercomputer when making such calculations for the entire Southern California Bight. In contrast, spectral-refraction models, such as that detailed in Dalrymple (1988), can be run on most personal computers. For these reasons it is often preferable to use spectral-refraction models and hence knowledge of their accuracy in regions of complex bathymetry is essential.

3. Applications to the Southern California Bight

The complicated bathymetry of the Southern California Bight, described in detail in Chapter II, makes it an ideal place to study the accuracy of wave transformation theory. Following Munk and Traylor's (1947) pioneering study, Shepherd and Inman (1950) linked the refraction of swell waves over the canyons to observed nearshore circulation patterns. Using dye and floats to observe the nearshore circulation, combined with visual observation of wave heights, and wave records from pressure instruments, it was shown that the nearshore circulation is largely driven by alongshore gradients in wave energy onshore of the canyons. Emery (1958) mapped wave trains in the Southern California Bights with aerial observations from a plane. Swell refraction was noted near the shores of the mainland and in the shallow waters near islands.

Spectral-refraction theory was first applied to the coastal waters of Southern California by Pawka (1983) to investigate sheltering of the California coast from swell by the Channel Islands. Pawka et al. (1984) compared spectral-refraction model predictions to array measurements in 10 m depth of water at Torrey Pines Beach, California (Figure 2). The predicted and observed spectra were in good agreement affirming that refraction and island blocking are the primary wave transformation processes in the Southern California Bight. O'Reilly and Guza (1991) continued the work of Pawka et al. (1984) by comparing a spectral-refraction model (Longuet-Higgins 1957) and a spectral refraction-diffraction model (Kirby 1986), over an analytical shoal and a region of simple bathymetry near Mission Beach, California. Later, O'Reilly and Guza (1993) furthered the comparisons by evaluating the two linear wave models over the entire Southern California Bight. Comparisons showed that in the deep, moderately exposed areas in the bight, the models were in good agreement. However in sheltered regions and areas of abrupt bathymetry, discrepancies were evident. Quantitative model validation was not possible due to a lack of concurrent coastal and deep ocean directional wave data, such as were collected recently at NCEX.

In preparation for NCEX, a pilot study was conducted with a limited array of sensors for 8 days in October 2002. Ray (2003) used the data to investigate wave transformation across the Scripps and La Jolla Canyon system. Analysis confirmed pronounced refraction of swell over the canyons and associated extreme nearshore wave height variations that were reported in Munk and Traylor's (1947) classic study. Ray (2003) compared the observations with a high-resolution spectral back-refraction model. The observed large spatial variations of wave energy and direction were well captured by the model with some discrepancies in regions of unusually low wave energy and steep bottom slopes. Although the results were encouraging, the short time span and small number of observation sites precluded a comprehensive verification of the model.

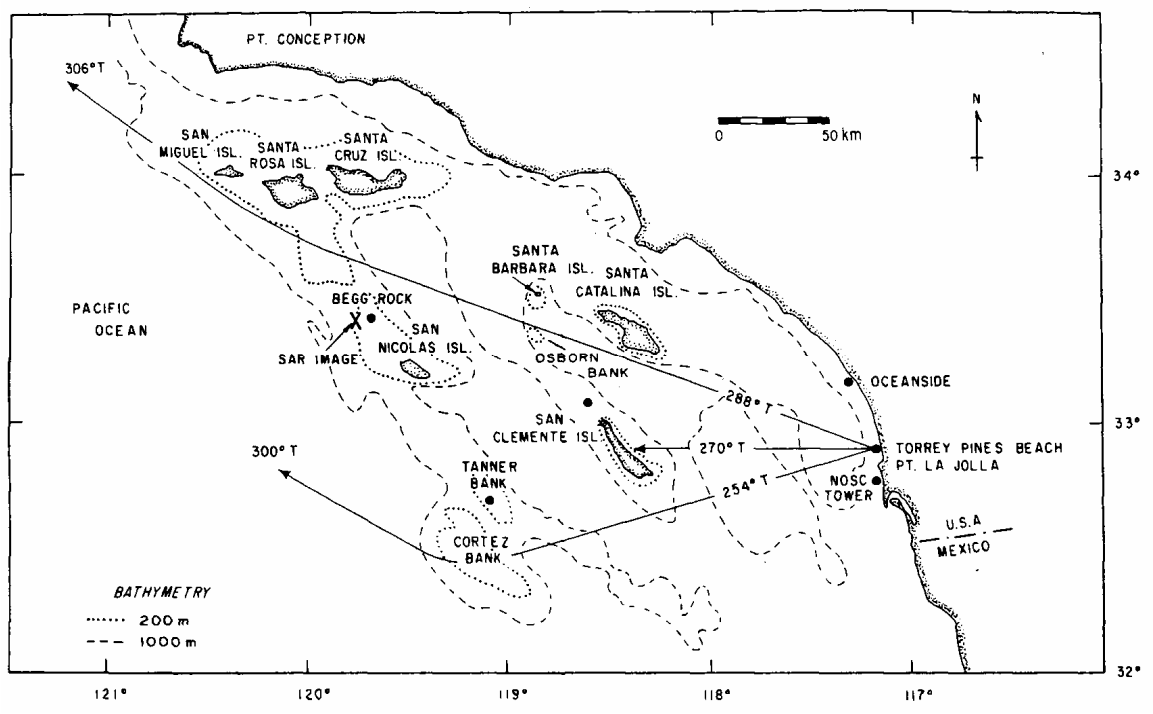

Figure 2. Southern California Bight showing 3 rays for 0.059 Hz waves incident to Torrey Pines Beach. (From: Pawka et al. 1984)

C. SCOPE

Previous studies have shown the accuracy of refraction theory in areas of slowly varying depth, and have presented qualitative agreement between linear refraction theory and observed refraction patterns over more abrupt bathymetric features, such as submarine canyons. The quantitative verification of refraction theory over complex nearshore bathymetry has not been reported, owing primarily to a lack of detailed field measurements. The availability of the extensive NCEX dataset, now make such a study possible. Therefore, this study investigates the accuracy of refraction theory for describing the (non-breaking) transformation of ocean swell across complex nearshore bathymetry. Specifically, the detailed measurements of swell transformation across the Scripps and La Jolla canyon system are used to test the robustness of the theory in a region with extreme wave variation.

Chapter II describes the NCEX experiment including data collection, the geographical setting of Scripps and La Jolla submarine canyons and the wave climatology of the region. Chapter III reviews methods used to analyze the field data. Chapter IV contains analysis of the observations. Refraction theory and model implementation are explained in Chapter V. Results of model-data comparisons are presented in Chapter VI, including overall statistics as well as individual cases studies of three significant swell events during the experiment. Finally, Chapter VII contains a summary and conclusions obtained from the research.

THIS PAGE INTENTIONALLY LEFT BLANK

II. EXPERIMENT

A. FIELD SITE

The Nearshore Canyon Experiment (NCEX) was conducted in the fall of 2003 near Scripps Institution of Oceanography in La Jolla, California. The institution is situated in the vicinity of two steep submarine canyons. Scientists from several universities and institutions conducted coordinated experiments to investigate nearshore waves, currents, sediment transport and other phenomena in a region with complex bathymetry. The present study uses data collected by instruments in 10-200 m depth to investigate the wave transformation over the Scripps submarine canyon, which is known to cause extreme variations in wave height along the coast.

Due to their close proximity to the Scripps Institution of Oceanography (SIO), Scripps and La Jolla submarine canyons are among the most extensively studied submarine canyons in the world. Figure 3 shows the coastline and underwater topography, with the study area marked by the red box. The coastline extends SSW from Blacks Beach approximately 2 km to the SIO Pier. Approximately 2 km beyond the SIO Pier, the coastline curves sharply to the west for approximately 1 km to Point La Jolla. Past Point La Jolla the coastline continues the NNE-SSW trend. It is known locally that the waves to the north of SIO Pier are usually small and increase dramatically farther north at Black's Beach, famous with surfers for large waves (Munk and Traylor 1947). Extreme variations in wave height (orders of magnitude) have been observed over alongshore distances of only a few hundred meters.

Scripps and La Jolla canyons form a deep Y-shaped chasm in the nearshore under- sea topography. La Jolla Canyon is the wider and deeper of the two and has an axis orientated NW–SE that extends to within 250 m of the shoreline. Scripps Canyon is comparatively narrower and extends NE-SW with its canyon head position within 200 m of Blacks Beach. The two canyons meet at a depth of about 300 m, and continue seaward to about 550 meters depth where they empty into the deep offshore San Diego Trough.

Ocean swell waves observed in the study area originate from storms over the Pacific Ocean in the northern and southern hemispheres, as far away as the Antarctic pack ice. Before reaching the submarine canyons of the study area, the waves must pass through the Southern California Bight, an area extending from 32ºN South of San Diego to 34.5ºN at Point Conception that contains numerous offshore islands and banks. Consequently, the wave climate of the Southern California Bight is among the most complicated of the United States (O'Reilly 1993).

In a classic study, Munk et al. (1963) examined the arrival of swell at San Clemente Island in the Southern California Bight. Using directional information from an array of three pressure instruments and linear refraction theory, the dispersive arrival of swell in the Southern California Bight was traced to individual storms around the globe. In the Northern Hemisphere, waves originating from directions north of 295º are blocked by Point Conception on the American mainland; and waves originating from directions east of 150º are blocked by Point Eugena, Mexico (Figure 4). This large swell window leads to significant seasonal variations in the dominant incident swell of the bight and commonly results in simultaneous arrivals of more than one swell with different defining characteristics. Typically, the dominant swell arriving in the winter months is from the north to northwest as a result from cyclones moving east through the North Pacific into the Gulf of Alaska or from cold fronts moving into the California coastal areas. In the summer months, incident waves mainly arrive from the south to southwest, created by winds from Northern Hemisphere Pacific anticyclones or from winter storms in the Southern Hemisphere and tropical storms in the Northern Hemisphere (Munk et al. 1947). However it must be noted that islands blocking the incident deep ocean waves, and the effects of the complex shelf bathymetry causes coastal wave heights to vary throughout the Southern California Bight and further restricts possible swell paths arriving at the study area (Pawka et al. 1984).

B. INSTRUMENTS AND DATA COLLECTION

During September 2003 a large array of wave and current recording instruments was deployed throughout the study area offshore of La Jolla, California, as part of NCEX. In total, 7 surface-following wave buoys, 17 bottom pressure recorders, 12 pressure-velocity sensors and 7 current profilers were deployed in depths ranging from 10-200 m (Table 1, Figures 5 and 6). In addition there were several permanent directional wave-rider buoys operating in the vicinity of the study area.

1. Buoy Observations

The permanently deployed Outer Torrey Pines and Point La Jolla Buoys, designated Buoy 100 and Buoy 095 respectively, were used to obtain measurements of incident wave energy and direction spectra in deep water. These buoys are part of a coastal monitoring network operated by the Coastal Data Information Program (CDIP) at SIO. The Outer Torrey Pines Buoy is located approximately 12.5 km west of Torrey Pines State Beach in 549 m of water and Point La Jolla Buoy is found approximately 6 km west of Point La Jolla in over 180 m of water (Figure 3). Seven additional buoys, designated sites 32 through 37 and site 39, were deployed in depths ranging from 23 to 111 m (Figure 5). Two buoys (sites 39 and 35) on the north side of the canyons were deployed to provide measurements of the incident swell arriving at the canyons from the northwest. Five buoys were deployed north (sites 33 and 34) and south (sites 32 and 37) of Scripps Canyon, and over the canyon axis (site 36) to measure topographic effects on swell passing over Scripps Canyon. All buoys were deployed and maintained by CDIP.

All buoys are Datawell Directional Waveriders, commonly used surface following buoys that measure wave height and direction spectra. The 0.9 m diameter buoy (Figure 7) is equipped with a 3-component accelerometer and a compass and tilt sensor. The buoys sample at a rate of 1.28 Hz and the data are processed by an onboard microprocessor into time series of horizontal (x,y) and vertical (z) buoy displacements as well as surface height and direction spectra. Spectra are processed every 30 minutes based on a 26 minute record length. The frequency resolutions of the spectra are 0.005 Hz in the range 0.025 Hz to 0.1 Hz, and 0.01 Hz in the range 0.1 to 0.58 Hz. Data are transmitted to shore via a HF radio link.

2. Bottom Pressure Observations

The 17 bottom pressure sensors were each mounted on a fiberglass bottom tripod fitted with an acoustic release attached to a recovery line with a pop up float to facilitate recovery (Figure 8). The deeper (>30 m) sensors were equipped with dual releases. All sensors were equipped with a precision clock to allow for coherent processing. They were deployed from the R/V GORDON SPROUL using differential GPS and special targeting software for precise positioning with accuracy to within about 5 m. The first group of sensors, designated sites 13-17, form a linear array along the 15 m depth contour south of the Scripps canyon head (Figure 5). The closely spaced sites 15-17 were positioned accurately (within 0.5 m) using underwater acoustic transponders. Sites 20, and 22-24 were clustered around the head of the Scripps Canyon (Figure 6) where the largest variation in wave parameters was expected. Site 21 was deployed approximately 1 mile to the north as part of a cross-shelf transect of instruments (Figure 5). Sites 25 through 31 were placed on the shelf between the La Jolla and Scripps canyons to measure swell transformation in a region strongly affected by both canyons (Figure 5).

The pressure sensors measure near-bottom pressure that is related to wave-height. The Setra Systems pressure transducer, through a well known linear transfer function, measures pressure via a stable electric circuit between a stainless steel pressure sensor, and an insulated electrode, separated by a variable capacitor. As the pressure increases, the capacitance decreases and the associated change in voltage is detected and converted into a DC output signal. Accuracy of the instrument is about ±0.1%. The pressure records were sampled continuously at a rate of 1 Hz and were internally recorded. The instruments were recovered every 4-6 weeks for a data turnaround, and redeployed at the same locations.

3. Pressure and Velocity (PUV) Observations

Sites 1 through 12 consist of Nortek Vector Current Meters (PUV) mounted on fiberglass tripods similar to those used for the pressure sensors. To aid recovery, sites 1-7 were fitted with acoustic releases and sites 8-12 were fitted with a polypropylene line and a surface float (Figure 9). These instruments were deployed in 10 m water depth to measure the alongshore variation in swell waves. Specifically, sites 1-6 were located in

the vicinity of the Scripps canyon head, where extreme alongshore variations in wave height were expected, while sites 7-12 were placed farther to the north.

The PUV contains a pressure sensor and a three-component acoustic Doppler current meter. Currents are measured by transmitting short pulses of sound and measuring the change in frequency (Doppler Shift) of the sound echo that is returned by reflections off particles suspended in the water column. The Vector probe consists of three receive transducers, each mounted inside a receiver arm, and a transmit transducer in the center. The central transmitter beam points vertically upward while the three receiver beams (displaced off to the side) are at a 60 degree angle relative to the vertical. Using the three receivers, all focused on the same sample volume located 15.7 cm above the transmit transducer, the three velocity components are obtained. The combined pressure (P) and horizontal velocity (U,V) data provide height and directional wave data equivalent to measurements of a pitch and roll buoy. The 'PUV' signals attenuate with depth and require a linear theory depth correction as described in Chapter III. The pressure and velocity time series were recorded internally in bursts with a record length of 136 minutes and at a sampling rate of 1 Hz, at 3-hour intervals. The instruments were recovered, turned around and re-deployed every 3 weeks.

4. Bathymetry

Dedicated bathymetry surveys of the nearshore canyon experiment area were conducted before and during NCEX. The data was distributed by Dr. Steve Elgar for use by NCEX investigators. A high-resolution bathymetry grid (1.5 second latitude and longitude) was assembled by Dr. Bill O'Reilly and Mark Orzech from various sources, including NOAA National Ocean Survey (NOS 1937,1972) data for the La Jolla region, RASCAL (2001) commercial swath surveys of both the north and south canyon branches, and a SIO partial swath survey of the canyons from the R/V New Horizon.

Site Number	Instrument Type	Latitude (Deg North)	Longitude (Deg West)	Depth (m)
1	PUV	32.8740	117.2543	11.10
2	PUV	32.8764	117.2550	11.05
3	PUV	32.8775	117.2554	11.34
4	PUV	32.8781	117.2554	10.12
5	PUV	32.8792	117.2562	9.87
6	PUV	32.8803	117.2574	10.10
7	PUV	32.8810	117.2578	10.05
8	PUV	32.8824	117.2580	9.67
9	PUV	32.8837	117.2583	9.84
10	PUV	32.8856	117.2585	10.16
11	PUV	32.8882	117.2588	9.98
12	PUV	32.8910	117.2588	10.17
13	Pressure	32.8728	117.2555	13.75
14	Pressure	32.8717	117.2560	15.11
15	Pressure	32.8709	117.2565	14.87
16	Pressure	32.8705	117.2567	14.79
17	Pressure	32.8703	117.2568	14.31
20	Pressure	32.8746	117.2561	26.60
21	Pressure	32.8910	117.2663	25.05
22	Pressure	32.8746	117.2575	28.02
23	Pressure	32.8762	117.2569	24.34
24	Pressure	32.8740	117.2556	23.33
25	Pressure	32.8690	117.2600	14.92
26	Pressure	32.8641	117.2625	14.99
27	Pressure	32.8613	117.2620	15.16
28	Pressure	32.8648	117.2672	25.69
29	Pressure	32.8655	117.2706	49.36
30	Pressure	32.8637	117.2600	10.24
31	Pressure	32.8667	117.2616	14.92
32	Buoy	32.8733	117.2565	23.99
33	Buoy	32.8738	117.2612	34.20
34	Buoy	32.8756	117.2575	23.10
35	Buoy	32.8789	117.2665	33.87
36	Buoy	32.8736	117.2576	111.35
37	Buoy	32.8723	117.2595	48.97
39	Buoy	32.8910	117.2690	35.06

Table 1. Instruments deployed during NCEX

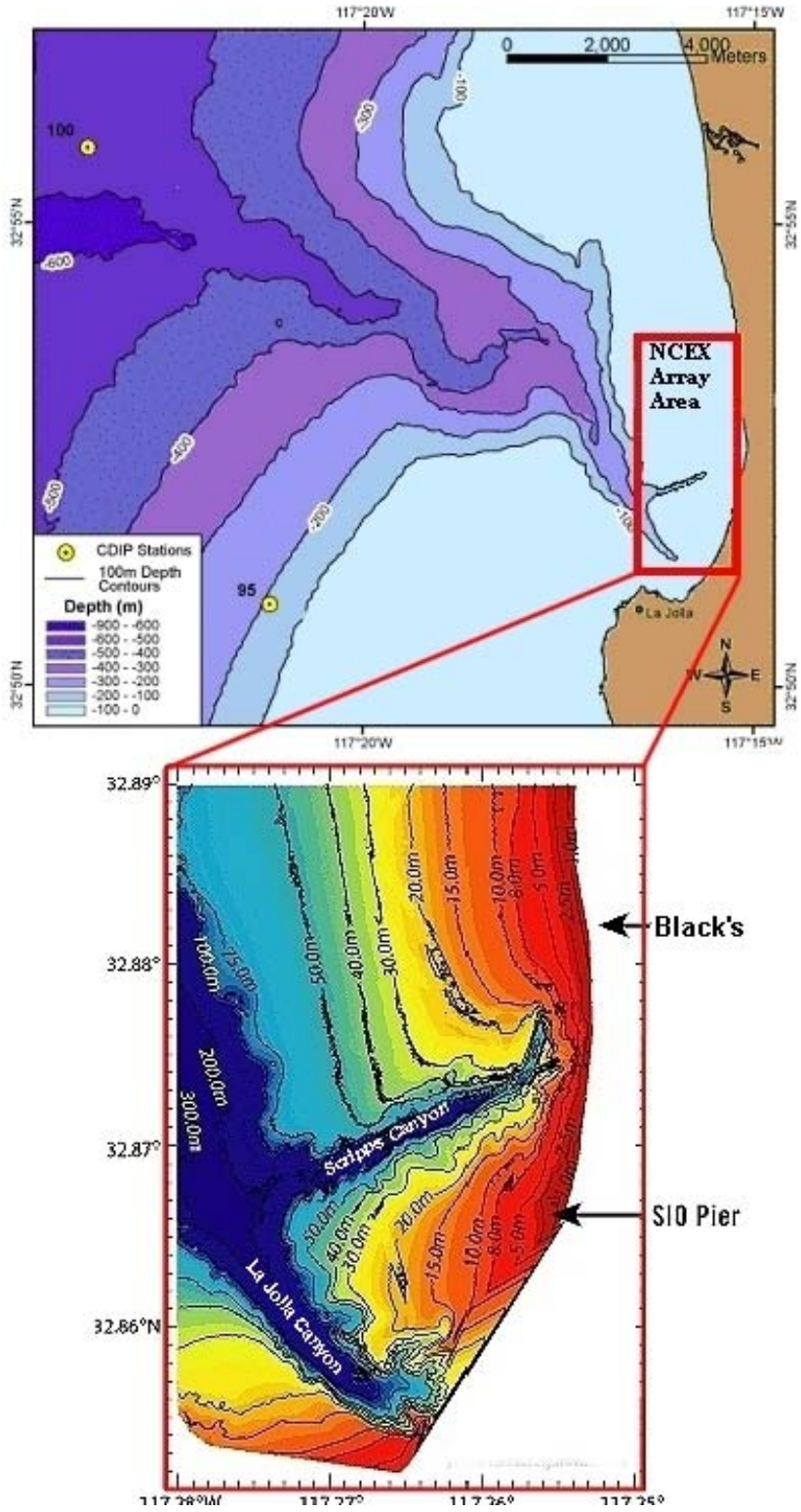

Figure 3. Bathymetry offshore of Scripps Oceanographic Institution including Scripps and La Jolla canyons (Bottom panel). The location of Torrey Pines Outer Buoy and Pt La Jolla Buoy are shown (Top panel) (adapted from: www.cdip.ucsd.edu)

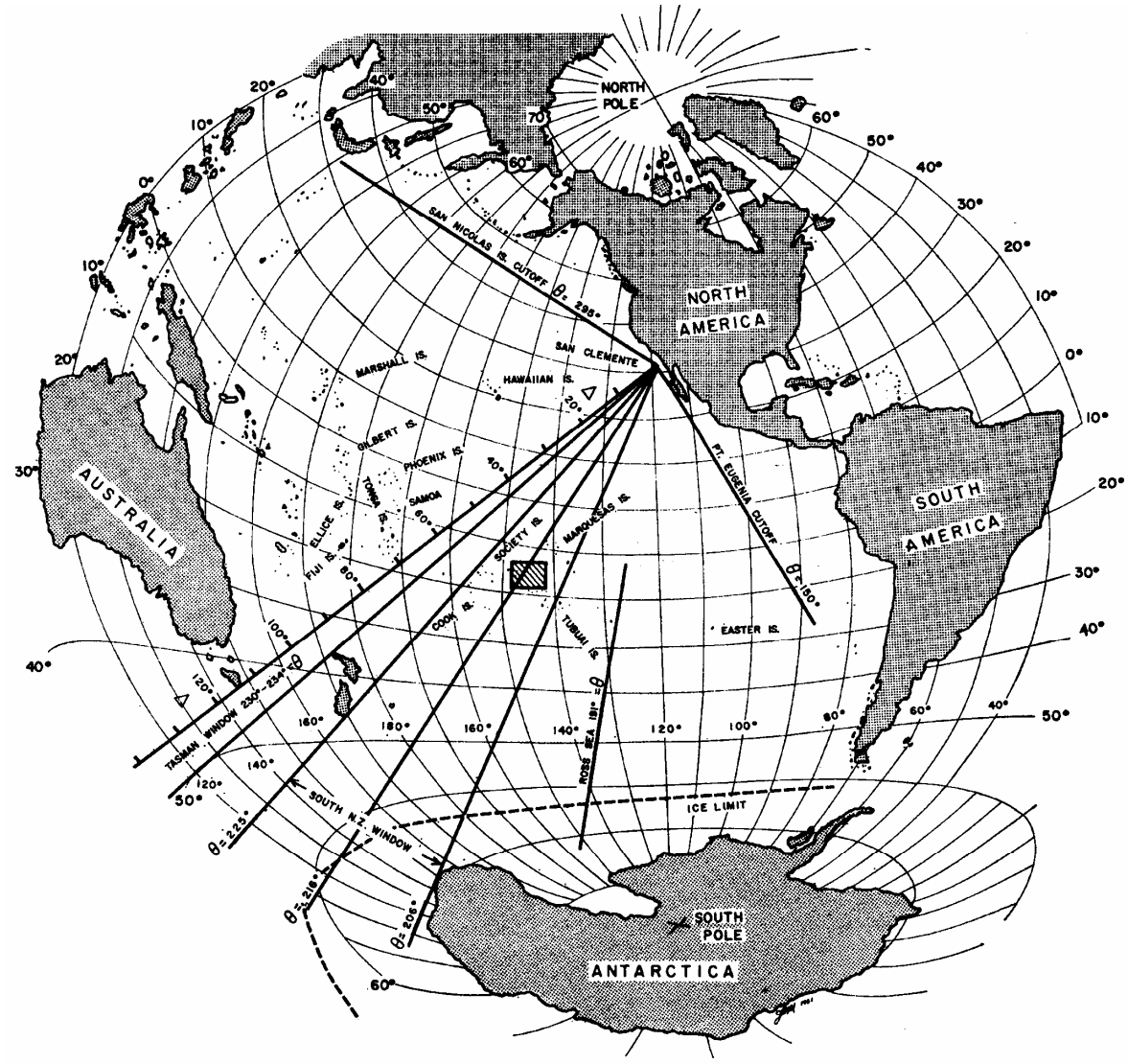

Figure 4. Azimuthal equidistant projection centered on San Diego, California, illustrating windows of possible swell propagation reaching the Southern California Bight from storms around the globe. New Zealand and Antarctic pack ice significantly limit swell paths from the storms centers in Southern Oceans. (From: Munk et al., 1963)

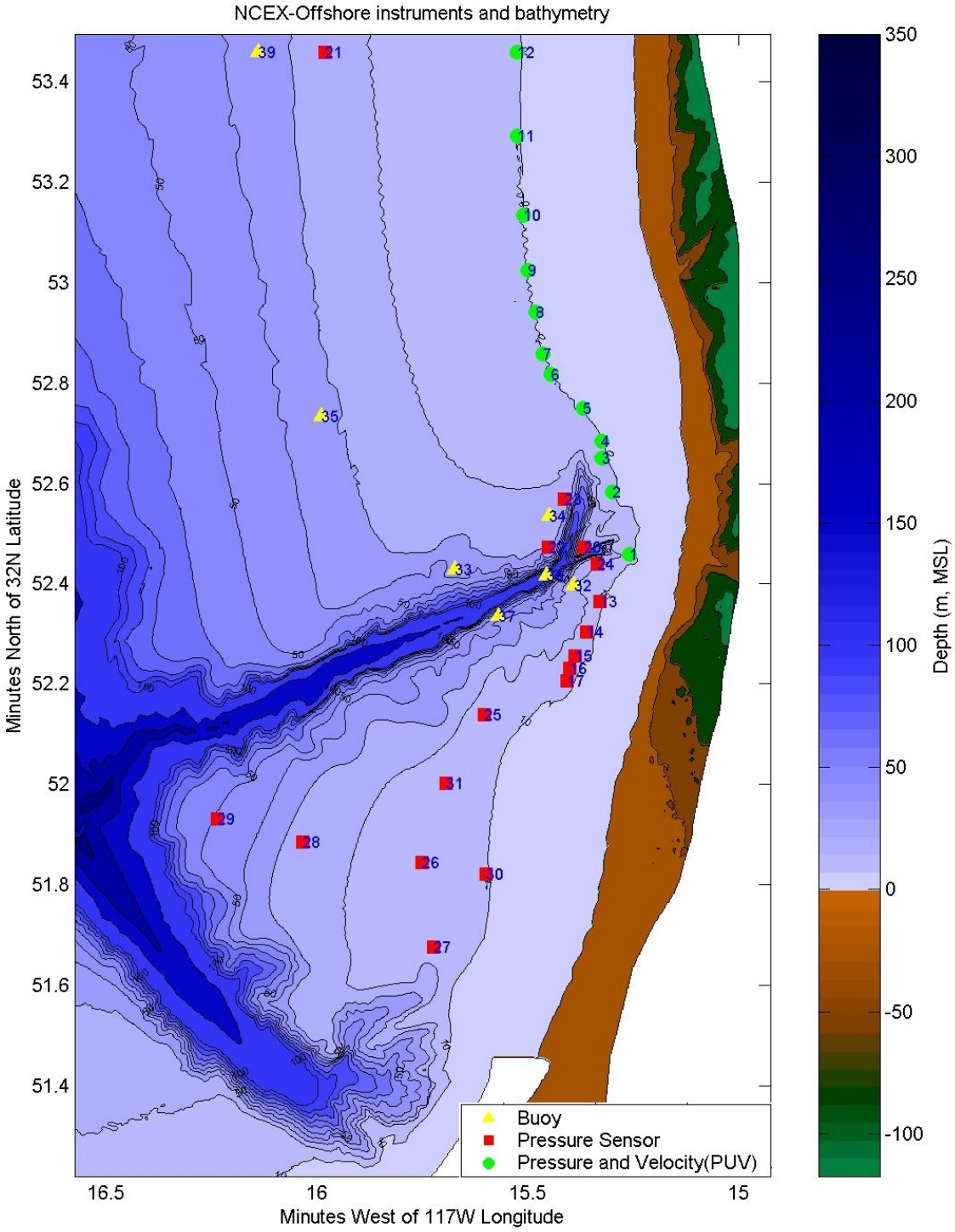

Figure 5. NCEX Instrument Array

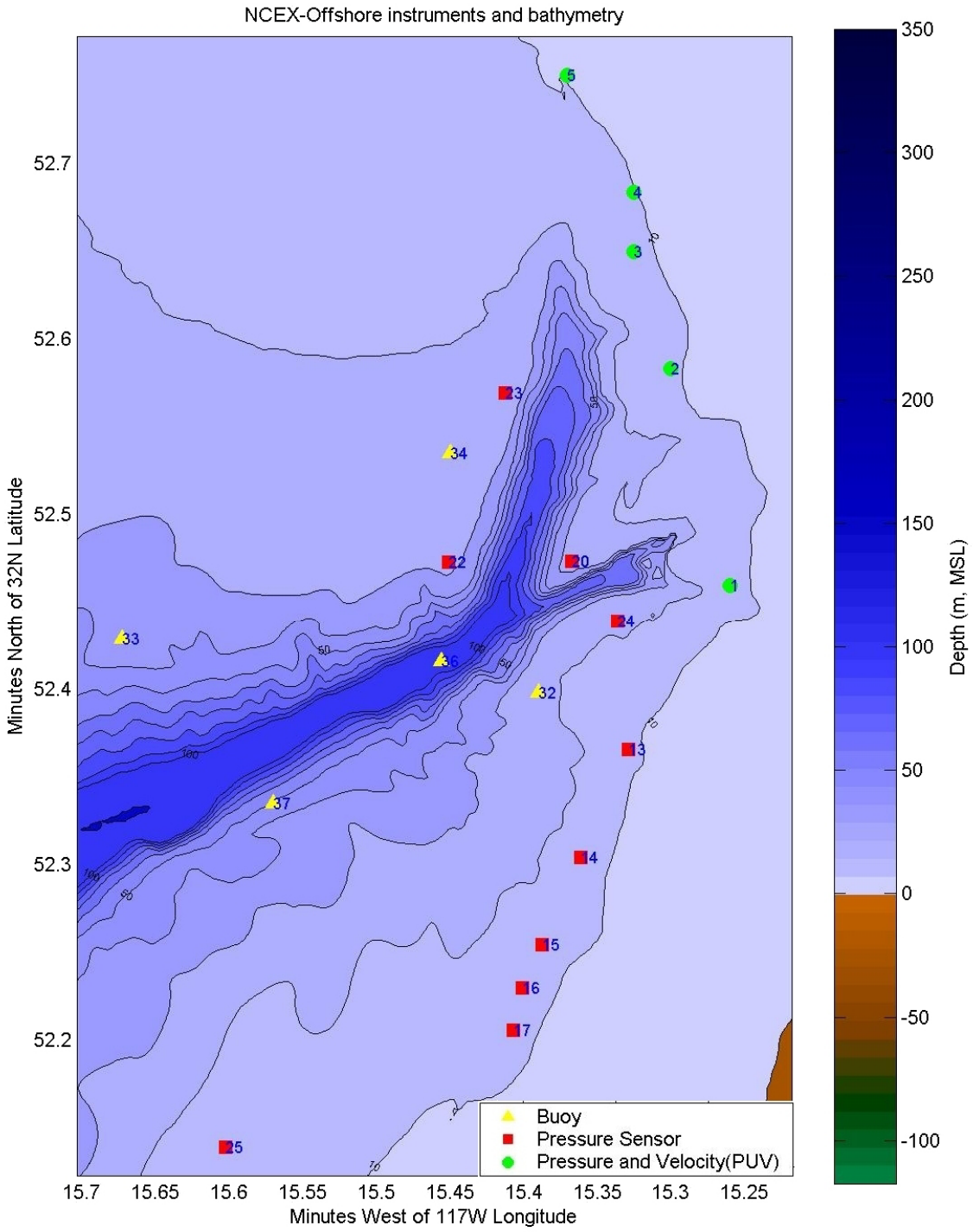

Figure 6. NCEX Instrument Array: Canyon Detail.

Figure 7. Datawell Waverider Buoy. This particular buoy is fitted with an anti-spin triangular frame to reduce the risk of damage from collisions. (From: www.cdip.ucsd.edu)

Figure 8. Pressure Sensor ready to be deployed during NCEX. The pressure sensor is mounted in a red fiberglass tripod equipped with lead feet to ensure stability on the ocean floor. Also shown are the two orange pop up floats each attached to an acoustic release to facilitate recovery.

Figure 9. Nortek Vector Current Meter about to be deployed during NCEX. Similar to the pressure sensor, the instrument is mounted in a red fiberglass tripod equipped with lead feet. The three receiver arms of the probe are seen above the left leg of the tripod, while the pressure sensor is located in the center of the instrument. A spare battery is located in the center of the tripod and a Nortek Aquadopp Velocity profiler is mounted near the rear leg.

THIS PAGE INTENTIONALLY LEFT BLANK

III. DATA ANALYSIS

The extensive array deployed in NCEX provided large datasets from several different types of instruments. This chapter details the techniques that were used to obtain frequency and directional wave spectra from these instruments, as well as common parameters such as significant wave height, wave peak period and mean wave direction.

A. DESCRIPTION OF THE WAVE FIELD

1. Surface Elevation Spectrum

In shallow water, bottom pressure sensors are routinely used to obtain sea surface elevation spectra. A subsurface pressure spectrum is readily converted to a surface elevation spectrum by applying a linear theory transfer function.

$$H_p(f) = \frac{\cosh kh}{\cosh kd} \tag{1}$$

where h is the total water depth, and d is the height of sensor above the seabed. The wavenumber k is given by the dispersion relation: $(2\pi f)^2 = gk \tanh kh$.

Considering the water column as a constant parameter linear system, the sea surface elevation spectrum then follows from multiplying the subsurface pressure spectrum by the squared transfer function.

$$E(f) = |H(f)|^2 E_p(f) \tag{2}$$

where $E_p(f)$ is the (input) pressure spectrum and $E(f)$ is the (output) sea surface elevation spectrum. For the NCEX experiment, surface height spectra were estimated from the pressure time series extracted from all PUV and P sensors.

The surface wave height spectrum is also calculated from the vertical motion of the waverider buoys. An onboard accelerometer measures the buoy's vertical accelerations that are then processed to yield a time series of the vertical displacement of

the sea surface. The auto-spectra (C_{zz}) of the vertical displacement time series thus yield a direct estimate of $E(f)$.

2. Frequency-Directional Spectrum

A full description of the spatial and temporal characteristics of a wave field requires knowledge of the wave frequency directional spectrum $E(f,\theta)$. In normalized form, the distribution of wave energy is defined as:

$$S(\theta;f)=\frac{E(f,\theta)}{E(f)} \tag{3}$$

The most common techniques for estimating the directional wave spectrum are based on the first four Fourier coefficients of $S(\theta;f)$, which can be derived from the horizontal and vertical displacements of a surface following buoy (Longuet–Higgins et al., 1963). Here we use the formulation of Long (1980), who showed that the first four Fourier coefficients of the directional distribution of wave energy can be expressed in terms of the spectra of the horizontal (x,y) and vertical (z) displacement time series.

$$a_1(f)\equiv\int_0^{2\pi}d\theta\cos\theta S(\theta;f)=\frac{iC_{xy}(f)}{\left\{C_{zz}(f)\left[C_{xx}(f)+C_{yy}(f)\right]\right\}^{\frac{1}{2}}} \tag{4}$$

$$b_1(f)\equiv\int_0^{2\pi}d\theta\sin\theta S(\theta;f)=\frac{iC_{yz}(f)}{\left\{C_{zz}(f)\left[C_{xx}(f)+C_{yy}(f)\right]\right\}^{\frac{1}{2}}} \tag{5}$$

$$a_2(f)\equiv\int_0^{2\pi}d\theta\cos 2\theta S(\theta;f)=\frac{C_{xx}(f)-C_{yy}(f)}{C_{xx}(f)+C_{yy}(f)} \tag{6}$$

$$b_2(f)\equiv\int_0^{2\pi}d\theta\sin 2\theta S(\theta;f)=\frac{2C_{xy}(f)}{C_{xx}(f)+C_{yy}(f)} \tag{7}$$

The PUV instruments produce the same directional moment information as that obtained from the waverider buoys. The horizontal velocity components u and v measured by the PUV are equivalent to the horizontal displacements x and y of the waverider buoys. The normalized co-spectra of (u,v) and pressure p, yield: (see Herbers et al. 1999)

$$a_1(f) \equiv \int_{-\pi}^{\pi} d\theta \cos\theta S(\theta;f) = \frac{C_{pu}(f)}{\left\{C_{pp}(f)\left[C_{uu}(f)+C_{vv}(f)\right]\right\}^{\frac{1}{2}}} \tag{8}$$

$$b_1(f) \equiv \int_{-\pi}^{\pi} d\theta \sin\theta S(\theta;f) = \frac{C_{pv}(f)}{\left\{C_{pp}(f)\left[C_{uu}(f)+C_{vv}(f)\right]\right\}^{\frac{1}{2}}} \tag{9}$$

$$a_2(f) \equiv \int_{-\pi}^{\pi} d\theta \cos 2\theta S(\theta;f) = \frac{C_{uu}(f)-C_{vv}(f)}{C_{uu}(f)+C_{vv}(f)} \tag{10}$$

$$b_2(f) \equiv \int_{-\pi}^{\pi} d\theta \sin 2\theta S(\theta;f) = \frac{2C_{uv}(f)}{C_{uu}(f)+C_{vv}(f)} \tag{11}$$

The directional distribution of energy $S(\theta;f)$ can be inferred from the first four Fourier moments by a number of different techniques (e.g. Longuet-Higgins et al. 1963, Long 1980, Lygre and Krogstad 1986). Here we use the Maximum Entropy Method (MEM) of Lygre and Krogstad (1986) to estimate the offshore frequency-directional spectrum of the outer Torrey Pines Buoy. This spectrum is used to initialize refraction model predictions presented in Chapter VI. It is often convenient to describe the directionality of waves by two simple parameters, the mean direction θ_{mean} and the directional spread σ_θ as functions of frequency. θ_{mean} is the mean of the directional distribution of wave energy, defining the dominant wave propagation direction at each frequency. σ_θ is the standard deviation of the distribution, which approximately defines the half-width of $S(\theta;f)$. If $S(\theta;f)$ is narrow then the mean direction and directional

spread can be estimated in terms of the first-order moments a_1 and b_1 (Longuet-Higgins et al. 1963, Kuik et al. 1988):

$$\theta_{mean} = \tan^{-1}\left(\frac{b_1}{a_1}\right) \tag{12}$$

$$\sigma_\theta = \left[2\left(1-\left(a_1^2+b_1^2\right)^{\frac{1}{2}}\right)\right]^{\frac{1}{2}} \tag{13}$$

Although not used in this study, θ_{mean} and σ_θ can also be defined in terms of the second-order moments a_2 and b_2 (see Herbers et al. 1999). Here we used equations (12) and (13) to estimate θ_{mean} and σ_θ (as a function of frequency) at all buoy and PUV sites.

B. SPECTRAL ANALYSIS

1. Wave Spectra Computations

In order to facilitate data comparisons, the data from each instrument was processed to yield spectral estimates over a common time interval. The waverider buoys produced 26-minute wave spectra every 30 minutes, the Vector current meters collected 137 minute bursts every 3 hours, while the p-sensors collected continuously. Therefore for each instrument, the spectral estimates were ensemble averaged over a 137-minute period commencing every 3 hours, with the exception of the short (4 minute) gaps in the buoy data. Thus all spectra are based on the same time. These 137 minute records are long enough that advection effects could be neglected (the travel time of 15 second swell with a 12 m/s group speed from the outer Torrey Pines buoy to the Scripps Canyon was approximately 20 minutes), and short enough that there was no significant tidal variation.

The directional moments, θ_{mean} and σ_θ, were computed from the ensemble averages of the directional moments $\left(a_1, b_1, a_2, b_2\right)$ weighted by the energy density $E\left(f\right)$. For each instrument site, this process yielded average wave spectra and directional moments at 3 hour intervals starting at 00:00, 03:00, 06:00, 09:00, 12:00, 15:00, 18:00, 21:00 hours Pacific Standard Time (PST) over the entire experiment period.

2. Bulk Parameters

In addition to full spectral estimates, the peak period T_p, peak direction, D_p, and significant wave height H_s were calculated. The dominant, or peak, wave period T_p and wave direction D_p, were taken as the period and mean direction corresponding to the frequency band with the maximum spectral density in the wave spectrum. The significant wave height was calculated using the conventional definition:

$$H_s = 4\sqrt{\int_{0.03\,Hz}^{0.1\,Hz} E(f)df} \tag{14}$$

where the spectral density, $E(f)$, is integrated across the swell frequency bands from 0.03 Hz to 0.1 Hz.

THIS PAGE INTENTIONALLY LEFT BLANK

IV. OBSERVATIONS

A. DEEP WATER WAVE SPECTRUM

The dominant swell in the Southern California Bight generally arrives from the south to southwest during the summer months and from the west to northwest in the winter months, as described in Chapter II. During the NCEX experiment, a wide range of offshore swell conditions was observed, capturing typical summer and winter swell events. Figure 10 displays a summary of these conditions measured by the CDIP Torrey Pines Outer Buoy. The significant wave height (over the swell frequency range 0.03-0.1 Hz) varied from 0.2 to 1.6 meters, with mean directions between 183 and 287 degrees, and peak periods between 10 and 20 seconds. The individual swell events can be more readily identified with a diagram that shows the energy spectral density versus frequency and time. The evolution of wave energy spectra for the month of October 2003 is displayed in Figure 11. Evident are the dispersive arrivals of swell from distant storms, whereby the long period swell waves arrive at the experiment area first, in the form of a narrow peak at low frequencies, followed by a progressive shift of this peak to higher frequencies, as the shorter period waves arrive. A clear example is displayed in the south swell event of 26-31 October.

B. WAVE HEIGHT TRANSFORMATION

Large spatial and temporal variations of wave height were observed in the NCEX study area. Figures 12 and 13 display the mean and standard deviation of the ratio of significant wave height at each instrument site to that offshore, for the entire experiment period. Evident is a large alongshore variation in wave height over the area (Figure 12), and extreme variation around the canyon head (Figure 13). To the north of the canyon at sites 6-12, wave height are relatively uniform, about 76% of the offshore wave height, with a small (0.14) standard deviation, indicating modest attenuation of the offshore wave energy associated with refraction over the approximately alongshore uniform shelf north of the canyons. At site 5 located just offshore of Blacks Beach, the highest wave heights are observed, on average approximately equal to the offshore wave height. The small standard deviation (0.14) indicates that both slightly amplified and slightly attenuated wave conditions are common at this site. Closer to the canyon (sites 2-4), wave heights

are smaller on average (68% of the offshore wave height), with larger standard deviations (about 0.23), demonstrating that these sites usually experienced moderate to strong attenuation of the offshore wave energy. Farther south there are large differences between sites. Onshore of the Scripps canyon head (sites 1, 20, 24, 13-17), wave heights are on average less than 30% of the offshore wave height, while on the seaward side of the canyon head (sites 22, 23, 33, 34), wave heights are more variable and comparable to the offshore wave height. These observations indicate that the canyon head acts as an effective barrier for the incident swell. Site 1 displays the most extreme attenuation, with on average 13% of the deep water wave height. At sites inshore of the canyon head standard deviations are small, indicating that they only receive a small fraction of the offshore wave energy at all times. Site 36, located directly over the canyon, shows similar small relative wave heights. Farther to the south, between Scripps and La Jolla canyons (sites 26-31), wave heights gradually increase to about 60% of the offshore wave height (on average) at site 26 located about midway between the two canyon heads.

The large variations of relative wave height observed at some instrument sites are caused primarily by a strong dependence on the offshore swell direction and period. Figure 14 displays scatter plots of the ratio of significant wave height to that offshore versus the offshore swell peak direction at four instrument sites. Since the expected refraction effects are stronger for longer period waves with longer wavelengths, the data were separated into short (10-13 seconds) and long (13-20 seconds) swell records. At site 12, far north of the canyon, short period westerly swells were slightly attenuated, where as longer period westerly swells were less attenuated and even amplified slightly in some cases. The southerly swells (which usually have longer periods) were attenuated between 10-50%. At site 5 close to Scripps canyon, long period north-westerly swells were amplified considerably (up to 50%), while the shorter period waves show a pattern similar to site 12. Southerly swells experienced a wide range of amplification and attenuation. At site 2 located farther south and behind the canyon head, a strong directional dependence is noted in the scatter diagram for long period swells with strong attenuation (as much as an order of magnitude) of southerly swells and virtually no attenuation of north-westerly swells. The sheltering effect of the canyon head is most

pronounced at site 1 with wave heights ranging from a few percent of the offshore wave height for long period southerly swell to about 25% for short period westerly swell.

C. MEAN DIRECTIONS

The shallow water refractive effects of the canyon system are evident not only in wave height variations but also in the range of the dominant swell direction D_p at the various instrument sites in relation to the offshore wave field. Figure 15 shows the peak direction D_p recorded at 4 instrument sites. When the offshore direction was W to NW, site 5 recorded swell from approximately 260º, but when the offshore swell was from the SW, swell was only recorded from approximately 230º, indicating two main arrival paths. Site 3 being slightly more sheltered than site 5, recorded a similar pattern but the range of shallow water swell directions was further confined to between 230º and 250º. Site 34, the most exposed of the 4 sites, displayed the greatest range of swell arrivals, receiving swell from more north-westerly angles than the other sites. Farther inshore of the canyon walls, the aperture of swell arrivals was as small as a few degrees. In particular, site 32 just to the south of the canyon head, only received swell from approximately 270º, regardless of the offshore swell conditions. In Chapter V, these very different arrival patterns at nearshore sites are shown to be consistent with theoretical refraction paths.

D. DIRECTIONAL SPREADING

The directional spread about the mean direction was examined at each instrument site in relation to the offshore spread. Figure 16 shows the directional spread at four representative instrument sites. At all sites generally narrower spreads were observed compared to that offshore, consistent with the effects of swell refraction over a shelf. However, the sites located to the north and offshore of the canyon (sites 5 and 34), show a broader spread than those sites located inshore of the canyon (sites 3 and 32). Sometimes a larger spread was observed at the sites offshore of the canyon than in deep water, suggesting simultaneous swell arrivals from multiple directions, possibly multiple refraction paths. On the other hand, the narrow spread recorded at the sites sheltered by the canyon, suggest the arrival of a narrow beam rather than a broad wave field scattered from the canyon head.

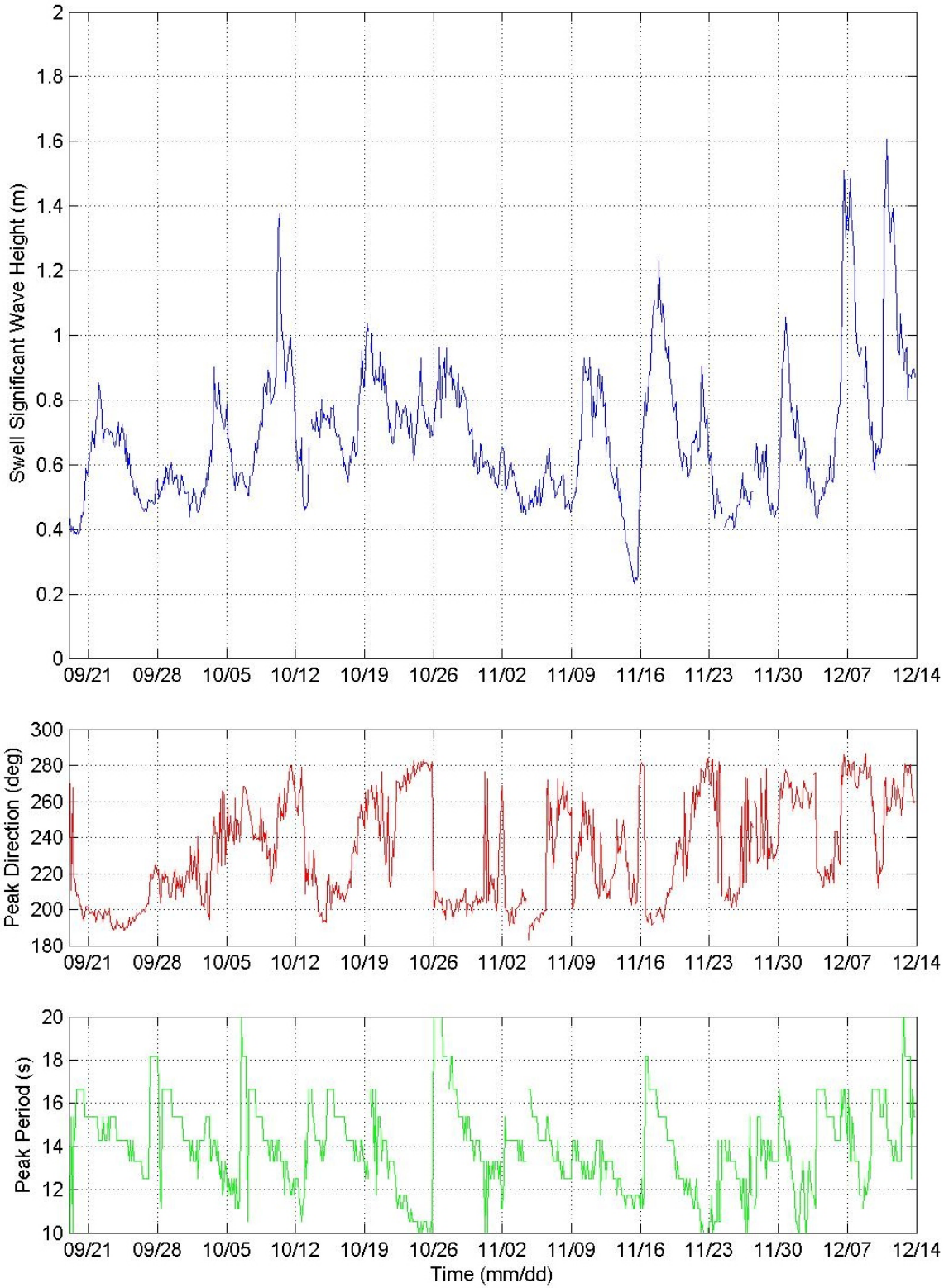

Figure 10. Deep water wave conditions measured at the CDIP Torrey Pines Outer Buoy

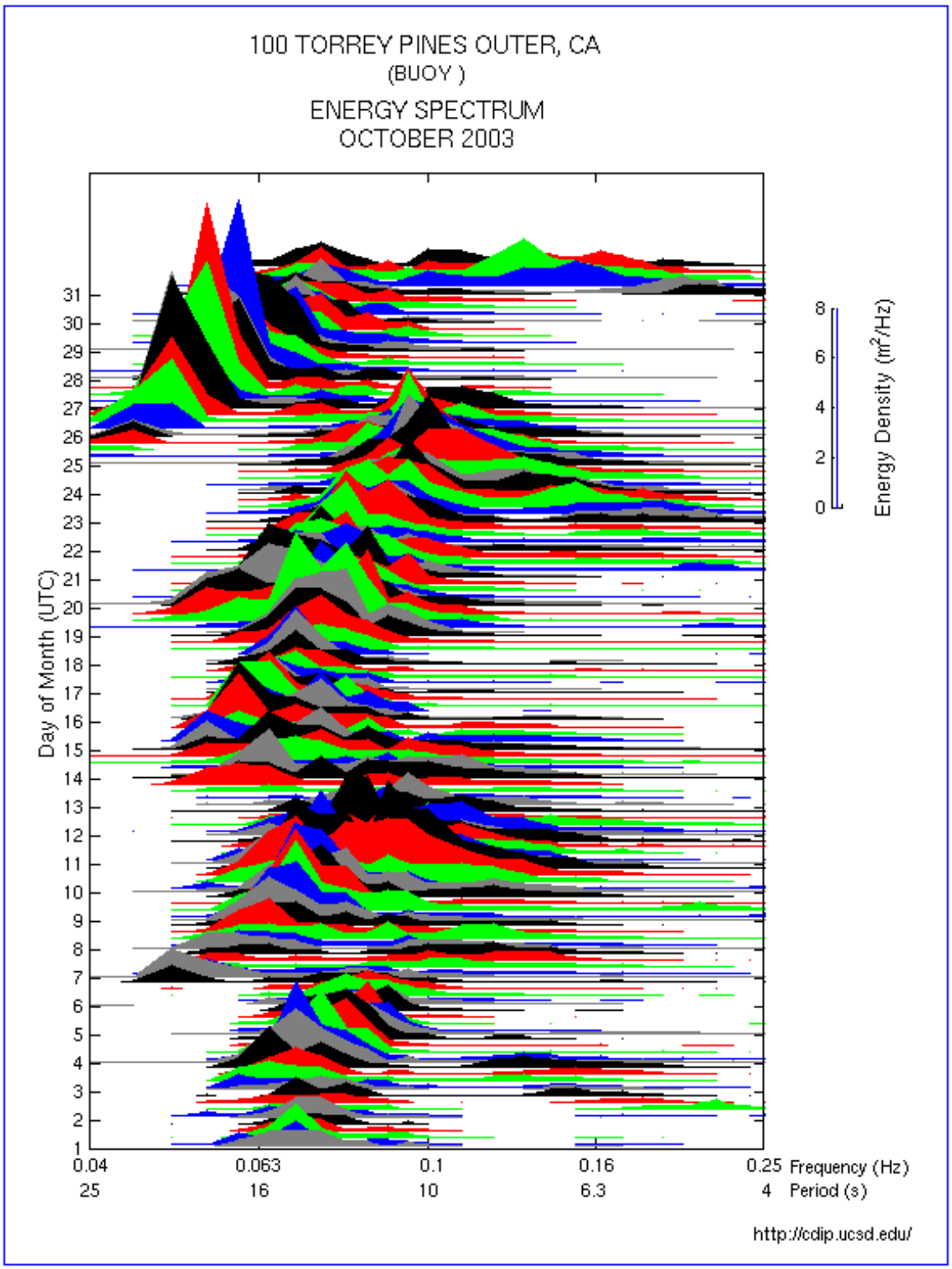

Figure 11. 3-hourly energy spectra measured at CDIP Torrey Pines Outer Buoy (Courtesy of Coastal Data Information Program http://cdip.uscd.edu)

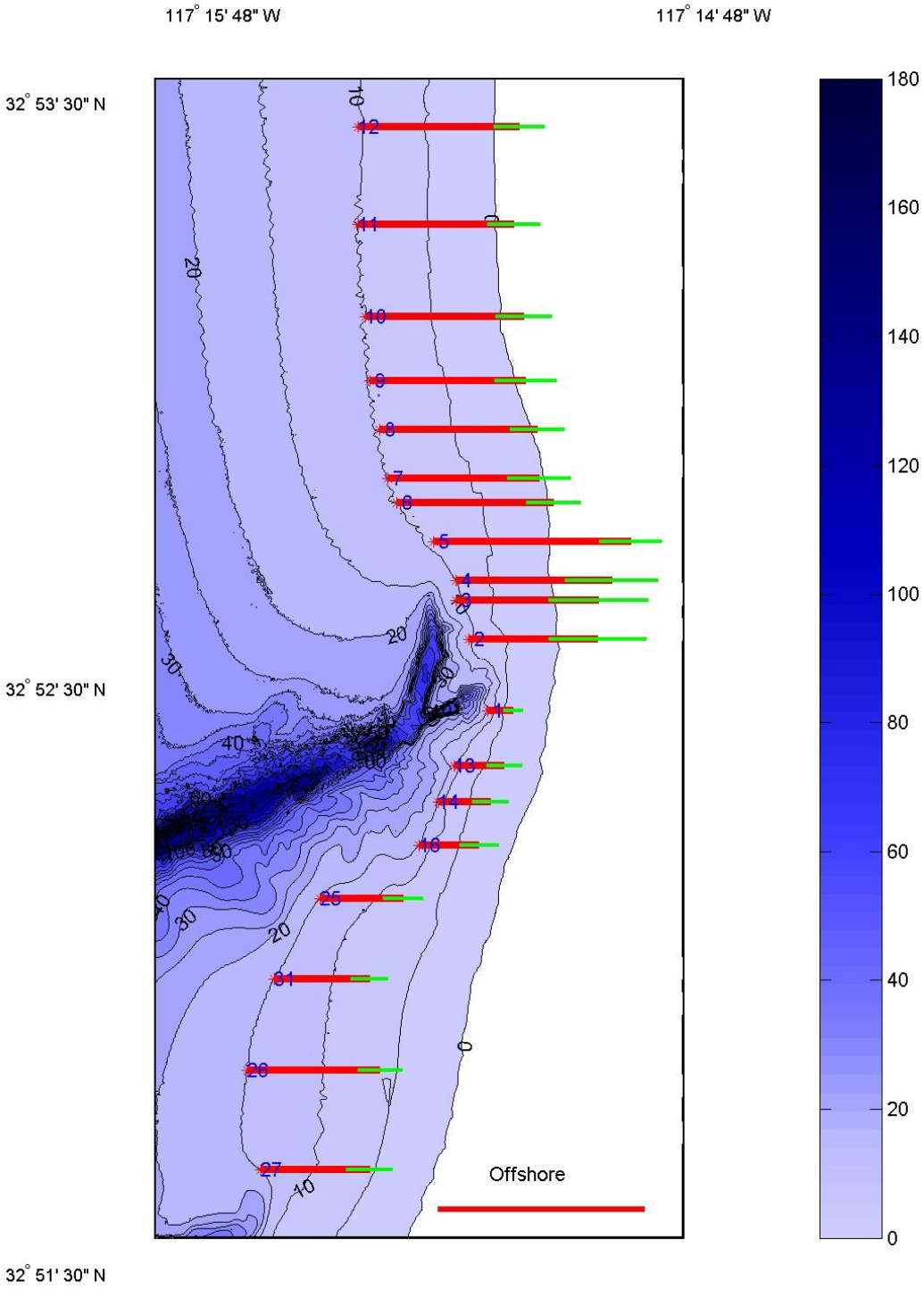

Figure 12. Mean and standard deviation of the significant wave height relative to offshore for the NCEX experiment period. The means are shown as red bars and the green bars represent +/- 1 standard deviation. Observations from instruments along the 10 and 15 m depth contours are shown to illustrate the strong alongshore variation near the head of the Scripps canyon.

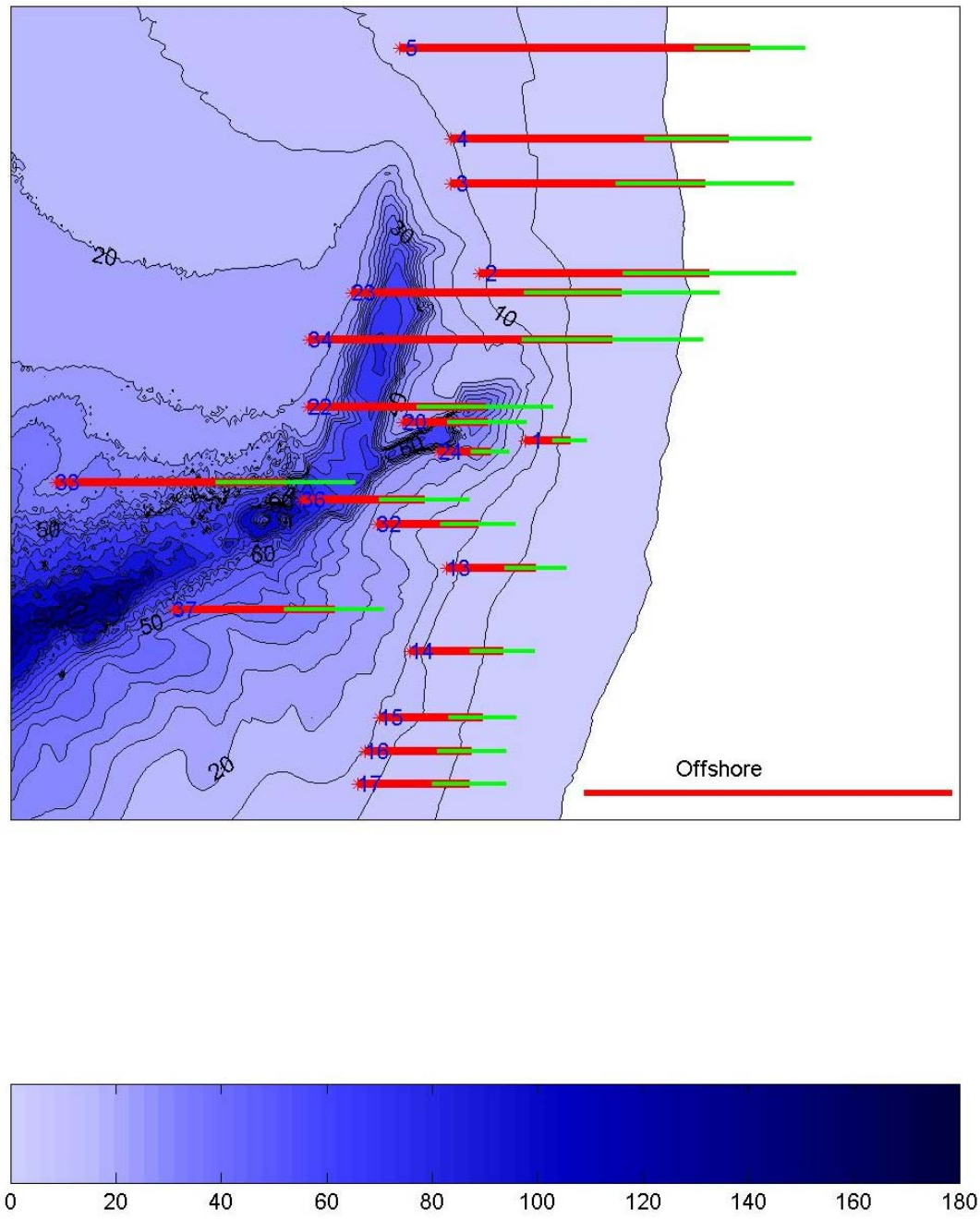

Figure 13. Mean and standard deviation of the significant wave height (relative to offshore) around the head of Scripps canyon. (Same format as Figure 12)

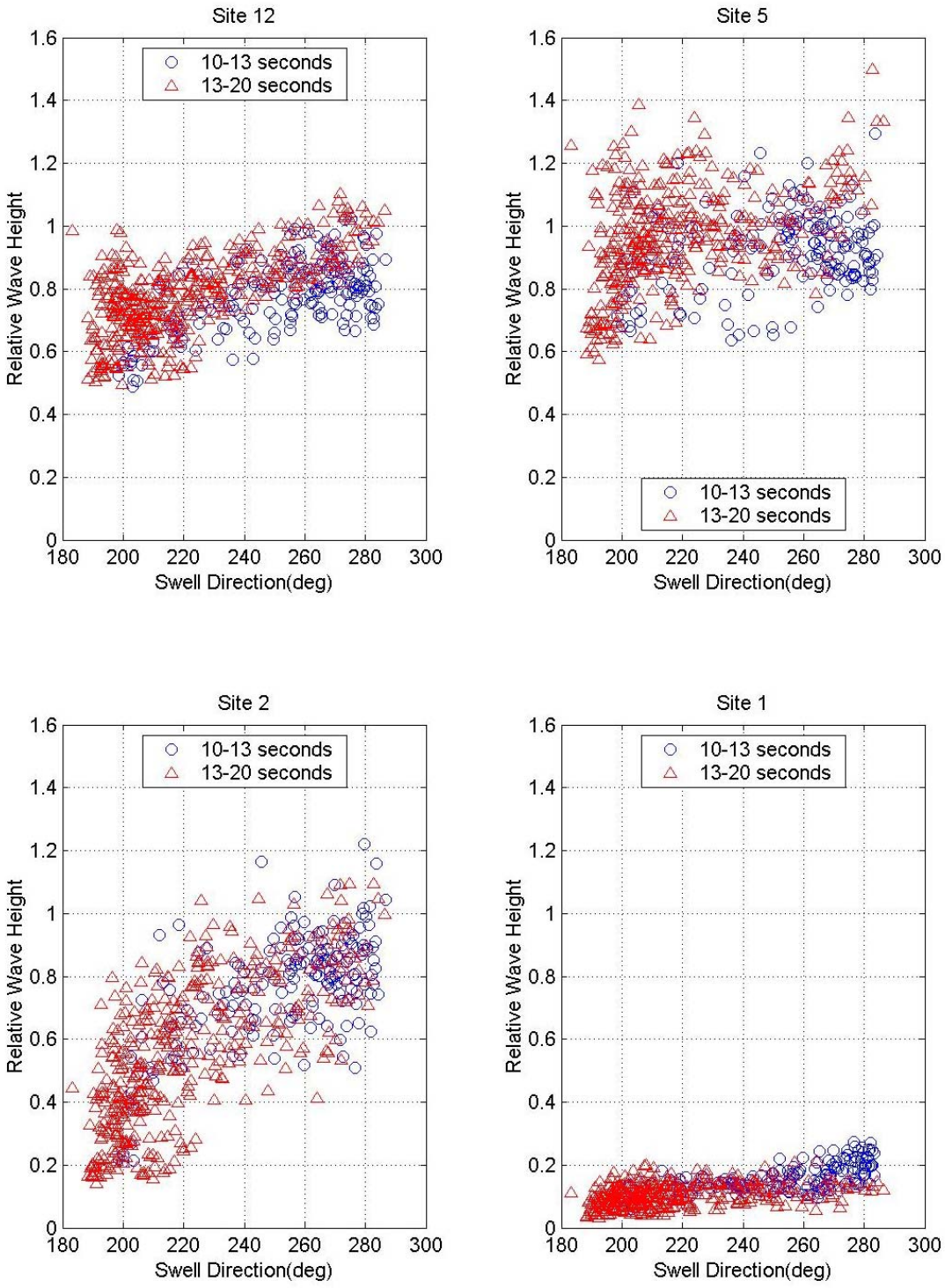

Figure 14. Ratio of significant wave height in shallow water to the wave height observed at the offshore Outer Torrey Pines Buoy versus offshore swell direction. Different symbols are used for short and long period swell observations. Results are shown for 4 different sites.

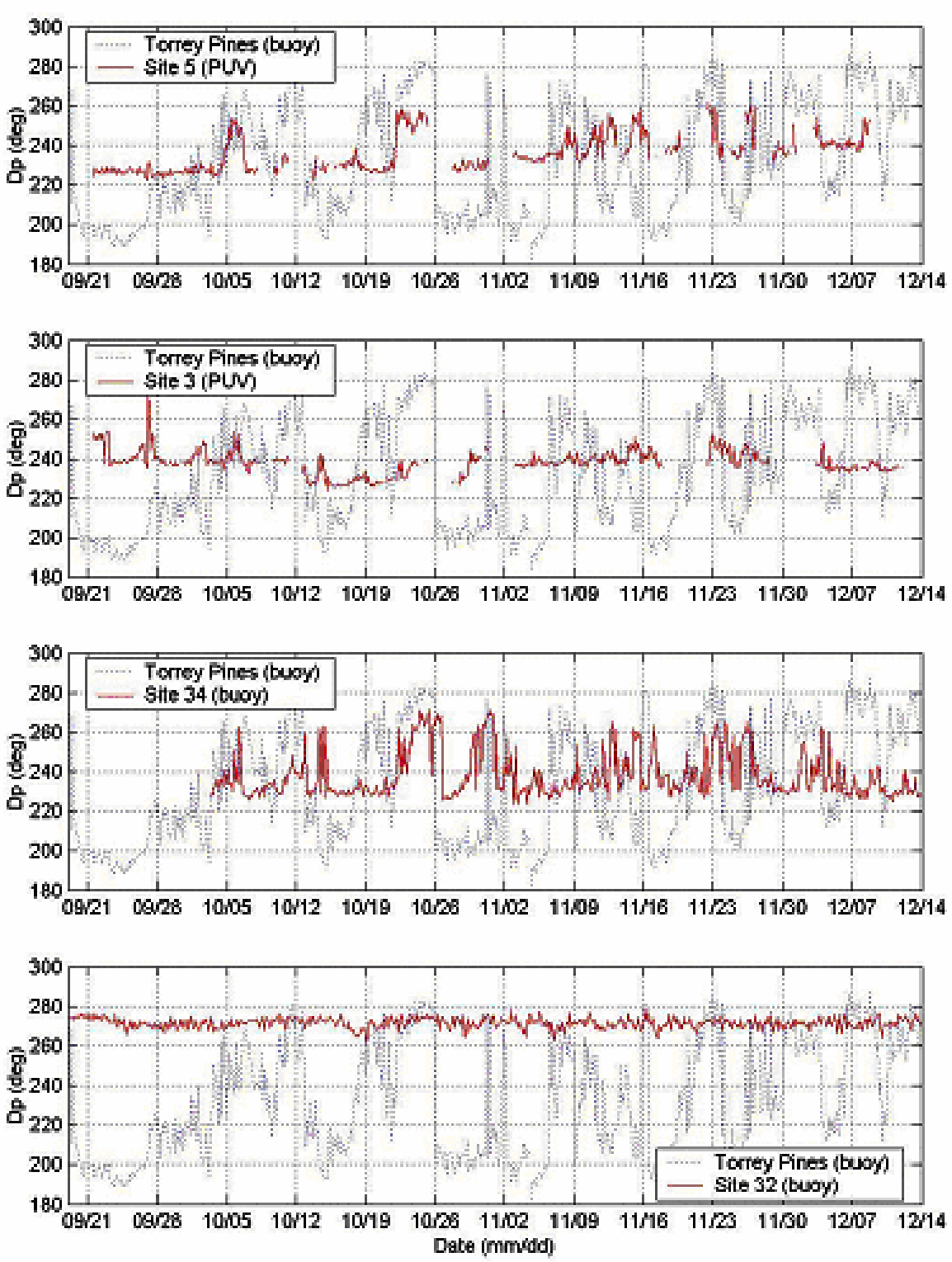

Figure 15. The peak swell direction (red) observed in shallow water is compared with the offshore directions (blue). Results are shown for the entire experiment period.

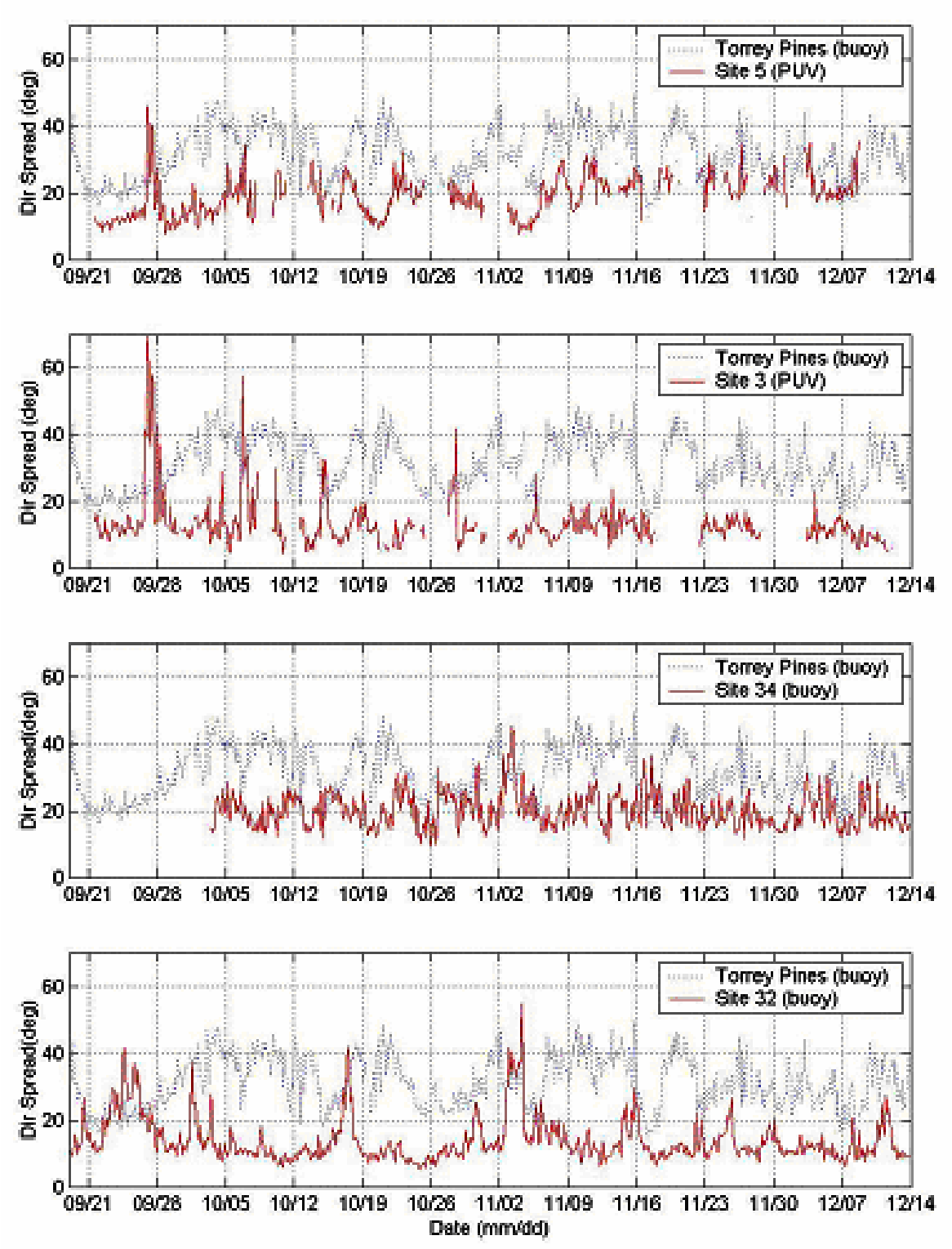

Figure 16. The direction spread (red) observed in shallow water is compared with the offshore spreads (blue). Results are shown for the entire experiment period.

V. RAY COMPUTATIONS

A. RAY THEORY

Wave refraction results from the dependence of wave phase velocity upon depth. As waves enter shallow water, the slower rate of wave advance causes the wave front to bend or refract towards shallower areas. For waves arriving at an oblique angle to the coastline, wave crests tend to become more parallel to the shoreline. This characteristic is analogous to the bending of light rays as they pass through media of differing refractive indices and can similarly be described by Snell's law of geometrical optics:

$$\frac{\sin\theta}{c} = \text{constant} \tag{15}$$

where θ is the angle between the wave crests and the respective bottom contours, and c is the phase velocity:

$$c = \frac{2\pi f}{k} \tag{16}$$

with the wavenuumber k given by the dispersion relation:

$$\left(2\pi f\right)^2 = gk\tan kh \tag{17}$$

It should be noted that the depth in which the wave velocity starts to decrease depends on the wave period. Thus longer period waves will be refracted in comparatively deeper water than shorter period waves.

The refraction of waves in more complicated regions with depth variations in 2-dimensions h(x,y), can be evaluated with ray theory, that is the construction of orthogonals (rays) to the wave crests that describe the propagation path of waves. Munk and Arthur (1952) developed a technique for tracing rays from deep to shallow water based on geometrical arguments. For an orthogonal Cartesian coordinate frame, the ray equations are:

$$\frac{dx}{dS} = \cos\theta \tag{18}$$

$$\frac{dy}{dS} = \sin\theta \tag{19}$$

$$\frac{d\theta}{dS} = \frac{1}{c}\left(\sin\theta\frac{dc}{dx} - \cos\theta\frac{dc}{dy}\right) \tag{20}$$

where s is the distance along a ray. These equations are readily integrated to determine ray trajectories. Plotting these ray trajectories can give a good visual indication of the wave transformation due to refraction. Since the energy flux between two rays remains constant, a convergence of rays indicates a region of wave amplification, whereas a divergence of rays indicates a region of reduced wave height.

To qualitatively describe the refraction of swell over the NCEX experiment area, ray trajectories were calculated based on Equations 18-20, for two typical swell arrivals (Figures 17 and 18). The bathymetry grid was obtained using Delaunay tesselation to create a faceted surface of triangles from the irregularly spaced depth soundings data, where the triangles are as equiangular as possible. The grid points were linearly interpolated from the surfaces of these triangles, with grid spacing of 3.91 m in the x direction and 4.63 m in the y direction. A ray step size of 5 m was used.

Figure 17 displays a ray diagram for a 16 second period NW swell arriving from 280 degrees. Waves arriving from north of the Scripps canyon axis are refracted to the north, resulting in an intense region of focusing just north of the canyon head

corresponding to Black's Beach. Waves arriving at the north wall of the canyon undergo stronger refraction than those waves arriving further north, resulting in crossing wave trains north of the canyon. Waves arriving south of the Scripps canyon axis are refracted to the south, providing a secondary region of focusing between the two canyons. The remaining area onshore and between the two canyons displays intense divergence and hence low wave energy. Farther south, the south wall of the La Jolla Canyon focuses wave energy onto Point La Jolla. The marked refraction for waves arriving closer to the canyon wall causes an area of crossing wave trains similar to that north of Scripps Canyon.

Figure 18 displays a ray diagram for a 16 second period SW swell arriving from 225 degrees. The ray pattern is similar to the NW case, with an area of convergence north of the canyon head and an area of divergence onshore of the canyon head. However, the high wave energy region in the vicinity of Black's Beach has moved farther north creating a wider region of low energy around the canyon head. A similar effect is found for the small focusing region between the canyons, showing that the entire refraction pattern has moved approximately 300-500 m north. In the southern areas, the rays arrive almost perpendicular to the La Jolla Canyon and cross onto the shelf between the canyons or are trapped on the shelf south of the Point La Jolla. This results in virtually no southerly swell reaching the Scripps canyon head and also less focusing onto Point La Jolla, than for a westerly incident swell.

B. SPECTRAL TRANSFORMATION

Longuet-Higgins (1957) showed that the ray equations can be applied to a continuous spectrum of waves to derive a direct relationship between the initially undisturbed spectral energy distribution $E_0(f,\theta_0)$, and the distribution after the wave field has undergone refraction $E(f,\theta)$. If diffractive effects are neglected, the relationship between the initial and refracted spectrum is described by:

$$E(f,\theta) = \frac{k}{k_0}\frac{c_{g0}}{c_g} E_0\left(f,\Gamma(f,\theta)\right) \tag{21}$$

where c_g is the group velocity and the subscript $_0$ refers to the incident wave spectrum before refraction. The inverse direction function, $\Gamma(f,\theta)$ describes the frequency-dependent relationship between the initial and refracted wave directions.

$$\theta_0 = \Gamma(f,\theta) \tag{22}$$

A practical technique to determine the transformation of a homogeneous deep ocean spectrum $E_0(f,\theta_0)$, to a shallow water coastal location (x,y), is to use the ray equations (equations 18-20) to construct rays through (x,y) for all possible frequencies and angles (f,θ) and determine the corresponding angle θ_0 in deep water. Next $\Gamma(f,\theta)$ is substituted into Equation (24) to yield the frequency-directional spectrum $E(f,\theta)$ at location (x,y). The numerical code for this backward ray tracing model was provided by Dr. William O'Reilly of the Scripps Institution of Oceanography and is described in detail in O'Reilly and Guza (1991,1993).

For the NCEX experiment area, the rays were back-refracted from each shallow water site to offshore. Figures 19 to 22 show the refracted rays from instrument sites to deep water. From the ray diagrams it is easy to discern the possible swell paths to each shallow water site. Site 5 is exposed to a wide range of swell arrival paths, including multiple swell arrival paths for a single offshore incidence angle (Figure 19). For example, for waves arriving from the west in deep water there is a direct path across the continental shelf to site 5 and also an indirect path that is strongly refracted over the north rim of Scripps canyon, arriving at site 5 from a south-westerly direction. This focusing of wave energy is consistent with the large amplification of wave heights at site 5 observed in Chapter IV. South swell arrives from direct paths only and any swell arriving further south than the canyons axis is refracted to the south, away from the canyon head. Site 34 exhibits similar westerly swell paths as site 5, but owing to its

location farther offshore it can receive swell from more northerly angles (Figure 20). However, any offshore direction greater than 295º is blocked by Point Conception (see Chapter II). In contrast to site 5, site 34 (closer to the canyon head) is sheltered from direct arrivals of southerly swells. This ray diagram is consistent with the amplification of westerly swells and attenuation of southerly swells observed at site 34 (Chapter IV).

The strong sheltering effect of Scripps Canyon is evident at sites located onshore and to the south of the canyon head, where relatively few ray paths extend to the open ocean. Both west and south offshore swells can reach site 32, however only along a narrow path that follows the Scripps canyon axis (Figure 21). Rays that propagate at an angle to the canyon axis are strongly refracted away from the canyon head. Hence only a small fraction of the swell energy reaches site 32 from a direction 280º that is in agreement with the observations (see Figure 15 in Chapter IV). This sheltering effect is most marked at site 1 (not shown), which exhibits no long period swell paths to deep water. Only short (<10 seconds) period swells reach site 1 by propagating unaffected directly across the canyon head.

Sites displaced sufficiently south of the Scripps canyon head are exposed to wave energy from direct paths across the deeper parts of the La Jolla Canyon. Deep water swell arriving at sites located between the two canyons, such as site 30, may also follow very complicated refracted paths. This is particularly true for longer period swells that may cross the shallow shelf off point La Jolla and or the walls of both canyons (Figure 22). It should be noted that all ray paths connecting offshore south swell to sites located in the southern part of the instrument array are not shown, because the model domain does not extend far enough south over the shallow shelf off Point La Jolla to connect these rays to deep water.

C. MODEL IMPLEMENTATION

The offshore directional wave spectrum was assumed to be homogenous everywhere and well estimated with the MEM method (Lyrge and Krogstad 1986) from data from the CDIP Outer Torrey Pines Buoy (see Chapter III). The same Delauney tesselation method described in earlier sections was used to generate the bathymetry field

for the model. Grid spacing was 38.0964 m in x-direction (east) and 46.30037 m in the y-direction (north). The resulting number of grid points was 289 in x and 272 in y.

First, wave rays were back-refracted from the shallow water instrument sites for all frequencies and in all possible directions to deep water. Along each ray, the local depth and bottom slopes were calculated using a second degree polynomial fit to the local bathymetry grid (Dobson, 1967) to determine the horizontal phase speed gradients. With these parameters, the ray back-refraction was performed using a fourth order Runge-Kutta method to integrate Equations (18-20). Initially, the inverse direction function, $\Gamma(f,\theta)$, was calculated by tracing rays for the full 360 degree range of possible starting angles using an initial angle step size of 1°. Rays were terminated upon hitting land or reaching the deep water boundary of the grid. Rays which reached deep water were then bisected with additional rays if the difference between the ending angles of two adjacent rays was greater than 0.5 degrees. This bisecting of starting angles continued until the 0.5 degree deep water criterion was met or until the difference between adjacent starting angles was less than 0.01 degree. O'Reilly and Guza (1991) liken this procedure to numerically integrating a function, with additional ray calculations performed where Γ varies most rapidly with θ. These ray computations were carried out for multiple frequencies (11 for 0.05-0.12 Hz, 5 for 0.12-019 Hz and 3 for 0.19-0.5 Hz), and the resulting transfer coefficients were averaged to model the wave transformation of 0.1 Hz frequency bands.

After the inverse direction function, $\Gamma(f,\theta)$, was established for a given shallow water site, the deep water frequency-directional spectrum was discretized into 1 degree bands with uniform energy density. Each 1 degree component was then transformed to the shallow water site using Equation (21) to obtain the shallow water spectrum. Finally the model generated energy and the first four directional moments with the same spectral discretization as the datawell directional buoy data (see Chapter II). Estimates of the bulk parameters were then made using those methods described in Chapter III. Time lags of the wave energy transmission between a deep water reference point and the shallow water sites were computed but neglected here in the transformation of the deep water spectrum to the shallow water sites, due to the small size of the model domain.

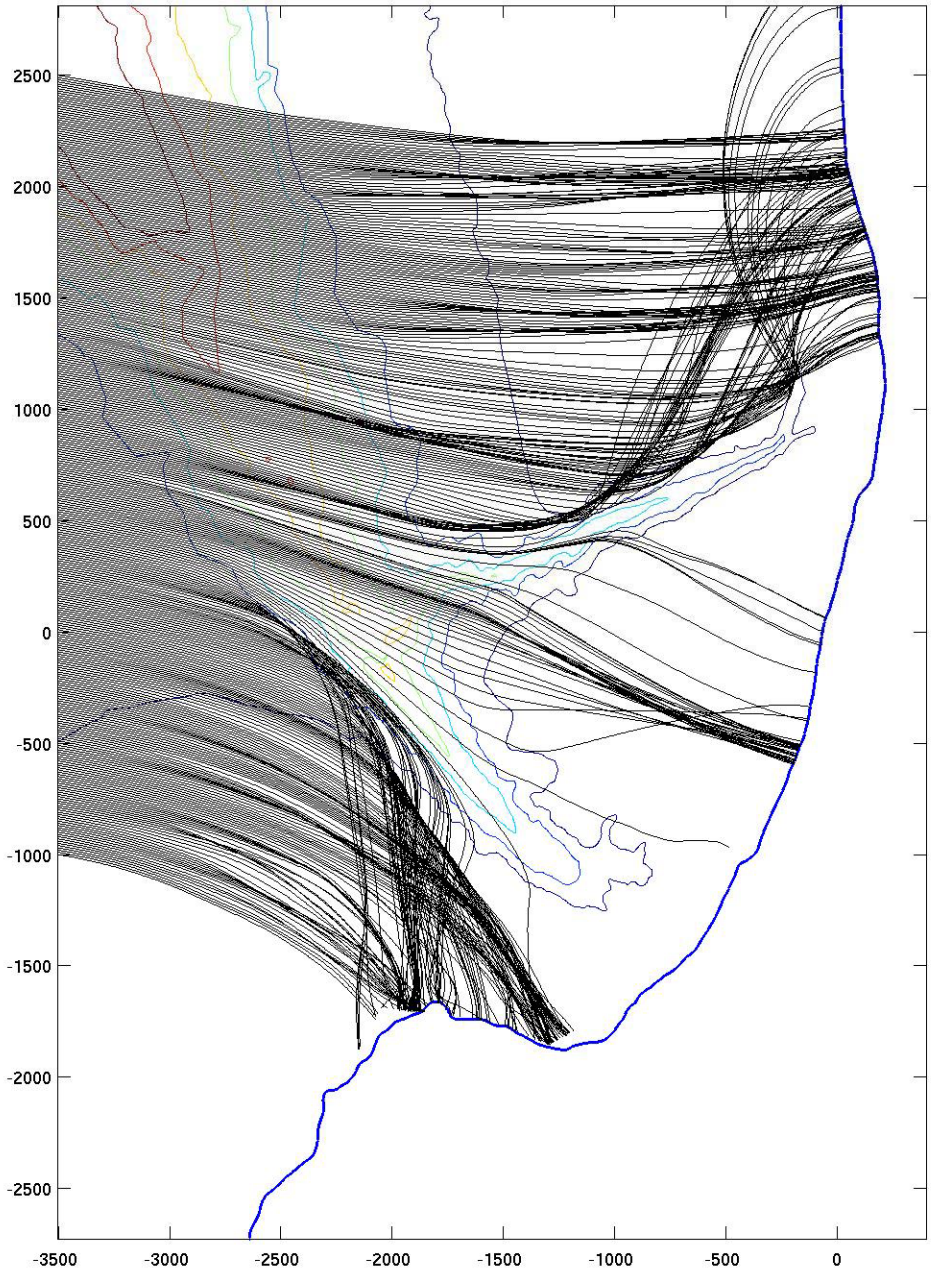

Figure 17. Ray trajectories for a typical west swell (16 second period, mean direction from 280˚). The spacing between rays at the offshore boundary is 10 m. The model domain is referenced to Scripps Pier (0,0) and distances are in m to the north (vertical axis) and east (horizontal axis).

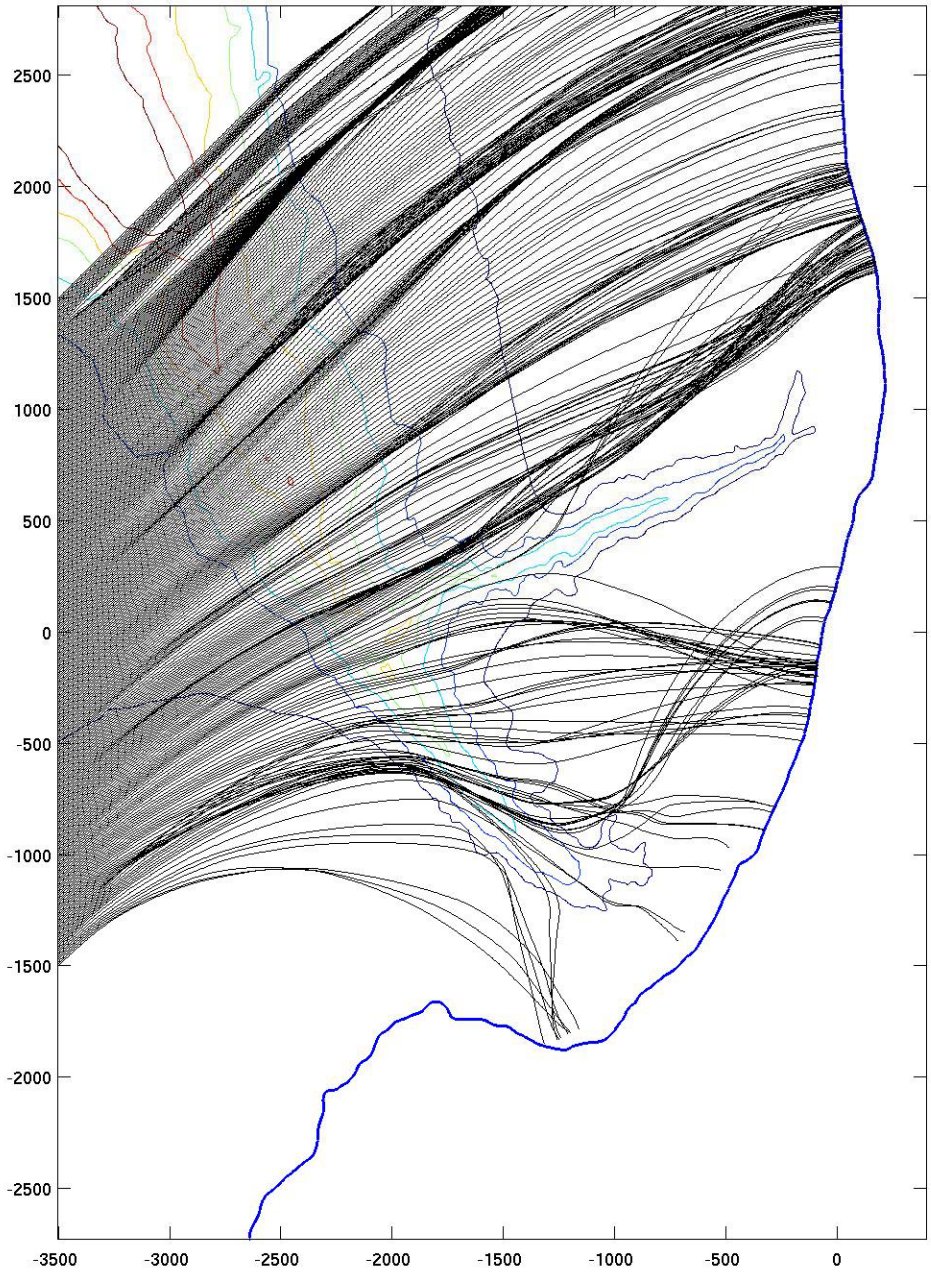

Figure 18. Ray trajectories for a typical south swell (16 second period, mean direction from 225˚). (Same format as Figure 17)

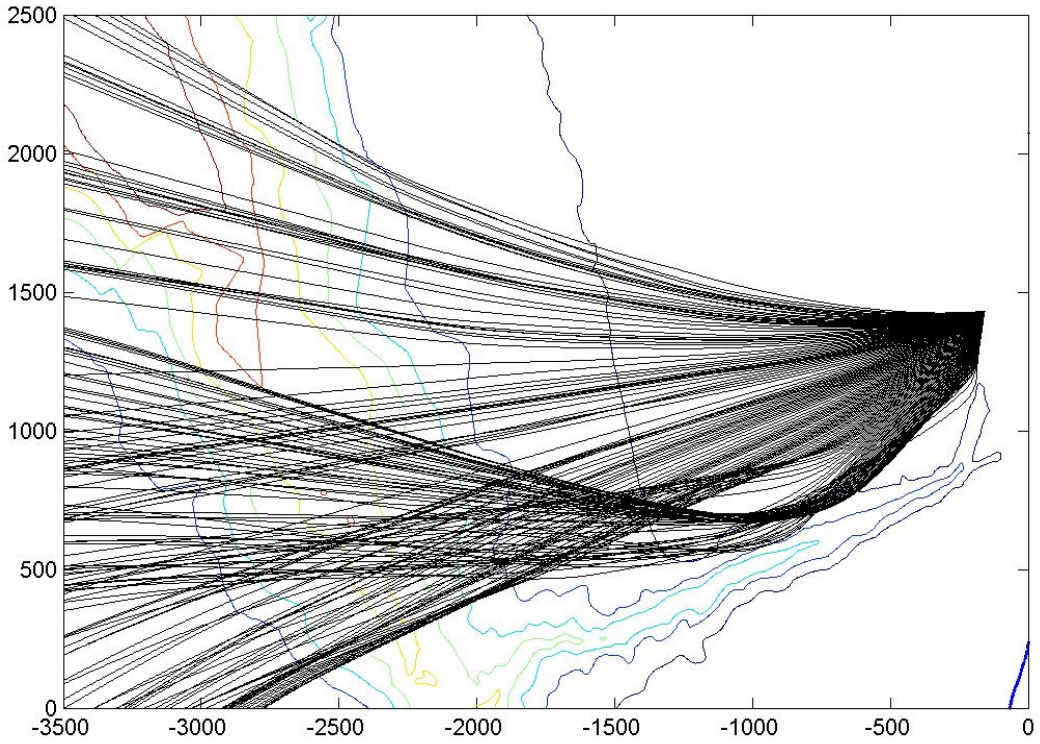

Figure 19. Rays for 14 second swell back-refracted from site 5 to deep water with a directional resolution of 0.5˚.

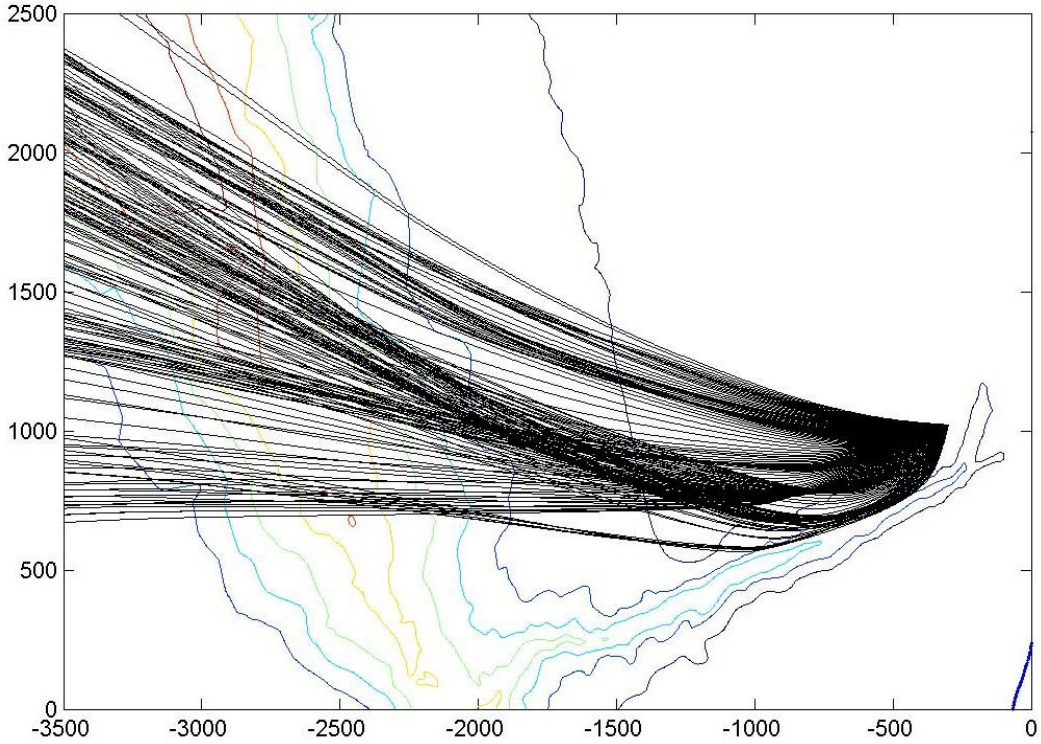

Figure 20. Rays for 14 second swell back-refracted from site 34 to deep water with a directional resolution of 0.5˚.

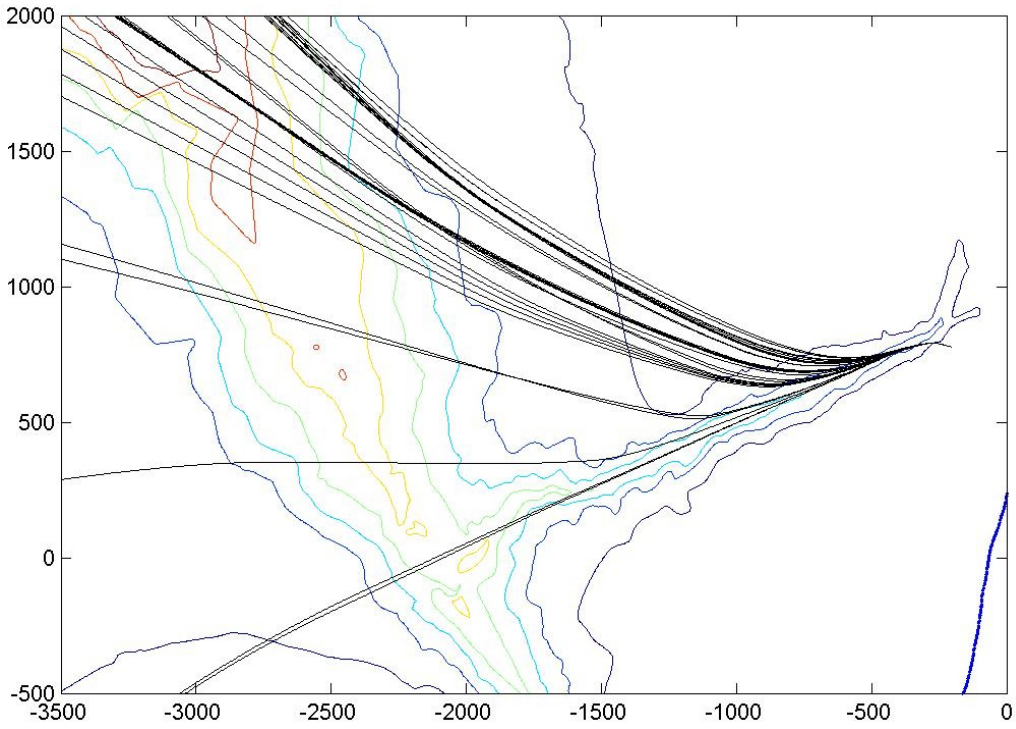

Figure 21. Rays for 14 second swell back-refracted from site 32 to deep water with a directional resolution of 0.02˚.

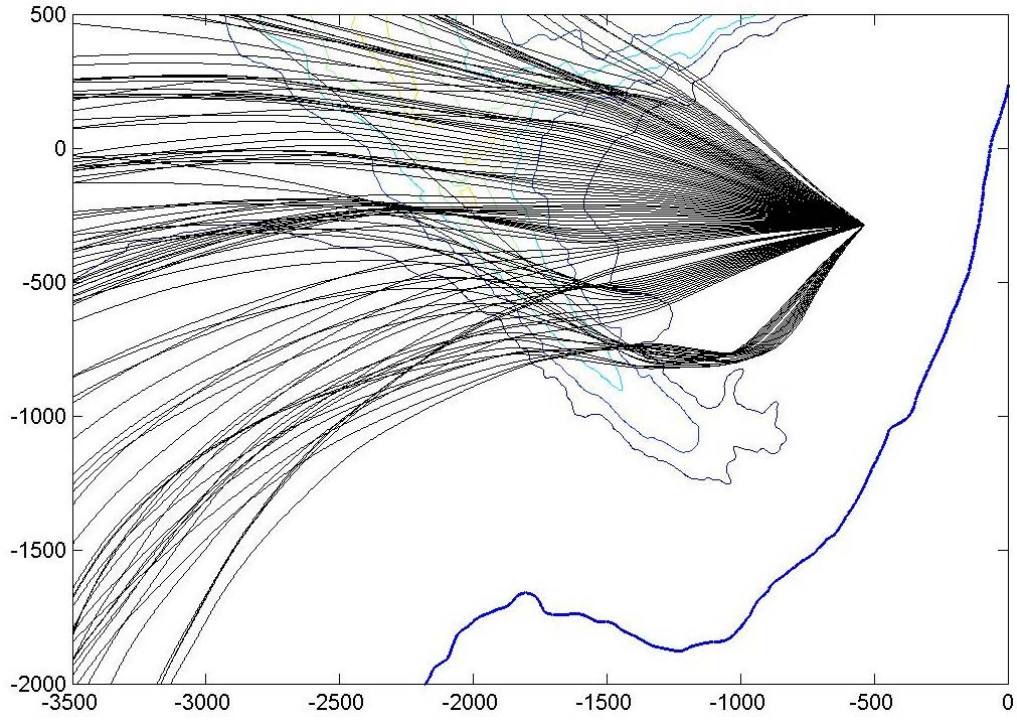

Figure 22. Rays for 14 second swell back-refracted from site 30 to deep water with a directional resolution of 0.5˚.

VI. MODEL RESULTS

Although the most commonly used regional wave models incorporate the process of refraction, their accuracy is limited by their ability to resolve the bathymetry in these areas, and their accuracy in regions of complex bathymetry is unknown. In this chapter, the accuracy with which refraction theory describes the transformation of swell across the NCEX area is examined through comparisons of predictions made with a high-resolution back-refraction model (described in Chapter V) with the NCEX wave data (described in Chapters II-IV).

A. MODEL-DATA COMPARISONS

To assess the accuracy of the linear refraction model, predictions of standard wave parameters were made for the entire experiment period at each instrument site. The model was initialized with estimates of the frequency-directional spectrum observed at the Torrey Pines Outer Buoy. These spectra were generally close to estimates at the Point La Jolla Buoy, with the exception of long period southerly swell that undergoes some refraction over the shelf offshore of the Point La Jolla buoy. Shallow water spectra predictions were made every 30 minutes, and then ensemble averaged over a 137-minute period commencing every 3 hours. The estimated directional moments, θ_{mean} and σ_θ, were computed from ensemble averages of the directional moments (a_1, b_1, a_2, b_2) weighted by the energy density $E(f)$. For each instrument site, this process yielded predictions of wave spectra and directional moments predictions at 3-hour intervals from 0000 PST 19 September 2003 to 0000 PST 14 December 2003.

The model predictions accurately reproduced the swell arrivals and associated temporal changes in wave height at all instrument sites over the experiment period. Figure 23 compares observed and predicted significant wave heights at two sites in the focusing region north of the canyon. The model correctly reproduces the large range of wave amplification and attenuation of the offshore wave height. As explained in Chapter V, site 5 almost always experienced amplified wave heights, particularly for offshore westerly swells due to refractive focusing, although southerly swells produced relatively lower wave heights, which arrived through direct paths only. Site 34 displayed a greater

range of wave heights due to very low wave energy conditions with southerly swells that are significantly sheltered by the canyon. The energy amplification associated with multiple swell arrival paths for westerly swells is slightly over predicted at both sites, while the attenuated southerly swells are under predicted at site 34. These discrepancies are possibly the result of neglected diffraction effects which tend to smooth out wave height gradients in focusing regions and contribute to the energy in sheltered regions that are blocked from direct swell arrivals along ray paths.

A similar pattern of agreement between model predictions and observations is noted in the low energy sheltered regions onshore of the canyon. Figure 24 shows results at site 1, which was sheltered from almost all offshore wave energy by the canyons and displayed the lowest wave heights of all sites at NCEX. Figure 24 also shows results at site 32 which is similarly sheltered from southerly swells but exposed to direct swell arrival paths for westerly swells (see Chapter V). At site 32 the model generally slightly under predicts the wave heights, whereas at site 1, the model over predicts the wave heights. Overall, the large wave height variations over the entire experiment period (including sites not shown in Figures 23 and 24) are well described by the model.

B. CASE STUDIES

Three data records were selected for further analysis. These three cases were chosen to span the range of offshore wave conditions described in Chapter II. The offshore frequency-directional spectrum for each case (estimated from the Outer Torrey Pines Buoy) is shown in Figure 25. All three cases are dominated by low frequency swell (peak periods 15.4-18.2 seconds) that are strongly affected by the canyons. The first two cases feature a narrow spectral peak corresponding to a single well-defined swell arrival, while the third case has a more complex spectrum owing to multiple swell arrivals. The case studies were selected to include both south and west swells during periods when most instruments recorded good data. Due to the required turnaround of instruments and the occasional instrument malfunction, a few sensors were not operational during each of these cases.

The observations presented in Chapter IV displayed strong alongshore variability that is of great importance to nearshore oceanographers as it can drive rip currents and coastal erosion. Any errors in the predictions of this variation will likely get amplified in

nearshore hydrodynamic and sediment transport models. Thus predictions made by the refraction model were examined with special emphasis on the alongshore variations close to shore.

1. Case I - West Swell 1200 PST 30 November 2003

Case I depicts typical offshore westerly swell conditions with a mean direction from 268°, peak period of 15.5 seconds and a significant wave height of 0.82 meters. Figure 26 compares observations and predictions of relative wave height $\left(Hs/Hs_0\right)$ at all nearshore sites, while Figure 27 compares observed and predicted frequency spectra at four different sites. The model over predicts wave heights to the north of the canyon (sites 5-12), where multiple swell arrivals cause a focusing of wave energy (see Figure 17 in Chapter V). The model accurately predicts wave heights at site 5 where the largest waves occur. However, a closer look at the energy spectrum (Figure 27) shows that this high level of agreement is somewhat fortuitous as the model slightly under-predicts the main low-frequency peak and over predicts at higher frequencies, yielding canceling errors in the wave height predictions. Toward the south as the sites become more sheltered by the canyons, this model tendency transitions to systematically under-predicting the wave heights, particularly at site 2. The observations show a large gradient in wave height between sites 2 and 13 that is apparently smoothed out by the model. It should be noted that site 1 (250m south of site 2) was not operational at this time, but very small wave heights would be expected at this site for these conditions (Figure 24). The energy spectra for sites 2 and 13 show that the errors are concentrated in the swell peak while spectral levels predicted at higher frequencies are in good agreement with observations. Moving further south, away from Scripps Canyon, the observed wave heights increase and the model predictions, while still slightly too small, increase in accuracy to site 26 located in the focusing region between the two canyons (Figure 17 in Chapter V). The intense divergence of rays caused by La Jolla Canyon, results in a smaller wave height at site 27. Hence the model under predicts the wave energy, particularly at the lower frequencies (Figure 27).

2. Case II - South Swell 1500 PST 28 October 2003

Case II depicts typical southerly swell conditions with an offshore mean direction from 203°, peak period of 15.4 seconds and a significant wave height of 1.0 m. The observed and predicted alongshore wave height variations are compared in Figure 28. The model accurately predicts the attenuation at sites 11-12 due to refraction over the shelf north of the canyon. At sites 6-8, the same over prediction is noted as for the westerly swell. The highest waves are again accurately predicted at site 5 and this is also reflected in the energy spectra (Figure 29). The gradient in wave height between sites 3-13 is not as abrupt as for westerly swell and well described by the model, in particular the very low energy conditions onshore of the canyon head at site 1. However, the low frequency swell peak is still attenuated too much in the model at site 2 (Figure 29). Farther south of the canyon wave heights increase and are accurately predicted as was the case for the westerly swell, but large errors are again noted at site 27, possibly owing to the proximity to the La Jolla canyon head and limited size of the model domain (see discussion below).

3. Case III - Mixed Swell 1200 PST 16 November 2003

Case III features a more complex incident wave field, with multiple swell arrivals. The narrow main swell peak features a mean direction of 197° and peak period of 18.2 seconds. A broader second swell peak exists with a mean direction of 277° and peak period 11.8 seconds. The offshore significant wave height (over the swell frequency range) is 1.4 m. A higher frequency third peak is outside the swell frequency range of the present analysis. Predictions of these high freqeuency waves are included in the energy spectra to illustrate the virtually undisturbed propagation of these shorter waves across the canyons. Figure 30 displays observed and predicted wave height variations along the shore. A similar pattern exists as for the previous two cases, with large wave heights up-and-downcoast of the canyon head, and small wave heights onshore of the canyon head. However, in this case the over-prediction north of the canyon is far more pronounced, particularly in the focusing region (sites 6-8). Spectral comparisons show that the main southerly incident swell peak is very narrow and hence diffraction effects not accounted for in the model may be more significant causing an over-focusing of wave energy at sites 8 and 5 (Figure 31). The broader higher frequency westerly swell peak is only

slightly over predicted and is consistent with predictions made for case I and case II. Consequently, the model predictions are heavily biased by poor handling of the narrow swell peak. This is also true for the focusing region between the canyons (site 26 in Figure 31). However, the model effectively shelters the instrument sites onshore of the canyon from the dominant narrow swell peak in agreement with the observations. Model predictions of the significant wave height in this region are quite good even though the predicted spectral levels of the 'blocked' low-frequency waves are well below the observed spectral levels (site 1 in Figure 31).

C. OVERALL MODEL PERFORMANCE

To quantify the overall performance of the refraction model during the NCEX experiment, a scatter index and bias defined as:

$$ScatterIndex = \frac{(\widehat{Hs}_{predicted} - \widehat{Hs}_{Observed})_{rms}}{(\widehat{Hs}_{Observed})_{rms}} \tag{23}$$

$$Bias = \left(\frac{\widehat{Hs}_{predicted} - \widehat{Hs}_{observed}}{\widehat{Hs}_{observed}} \right)_{mean} \tag{24}$$

were calculated for each instrument site over the entire experiment period. In order to give equal weight to high and low offshore wave conditions, the wave heights were normalized by the offshore wave conditions. Hence $\widehat{Hs}$ is the ratio of significant wave height at the instrument site to that offshore. The results are shown in Figure 32.

The scatter indexes show that on average the model predictions of the wave height are accurate to within approximately 20 percent. The errors are generally smaller at sites located further away from the canyons. This is most evident at sites 9-12, far north of the canyon, where the scatter index is about 0.15. In contrast, at sites 1 and 20, the two most sheltered sites, the scatter index is 0.33. These sites are also located very close to the canyon walls, where diffraction effects may be important. Another possible source of errors is inaccuracies in the bathymetry grid. A closer examination of the

model at site 20, revealed that the proximity of the canyon distorted the polynomial surface that the model fitted to the bathymetry grid to obtain depth gradients used in the refraction calculations. However, predictions made for this site with increased grid resolution (3.91 m x and 4.63 m in y) observed no significant gains in model accuracy. Other sources of error may include positioning errors in deployment of the instruments and navigational inaccuracies in the bathymetric surveys. However, such errors tend to be hard to identify and correct.

The largest scatter index occurs at site 27 located close to the La Jolla canyon head. The limited model domain size may contribute to this error, as site 27 is located near the southern boundary of the model domain. For rays to reach this site, they must undergo extreme refraction (more than 120º) over the shallow shelf off Point La Jolla. It is possible that there are ray paths that travel a long distance along the shelf before reaching deep water well outside the model domain boundary, and the energy carried along these rays is not included in the predictions. Thus the model may not be able to propagate enough energy into site 27, particularly for south swells, and this is consistent with the large negative bias for this site (Figure 32).

It also appears that predictions for the buoy sites generally are more accurate than those at the pressure sensor and PUV sites. This may be due to the buoy drift circle, which in effect averages observed wave conditions over a finite region in contrast to sensors deployed on the seafloor at fixed locations. This effect may be significant close to the canyon where bathymetry effects are most severe. Additionally, bottom pressure measurements close to the steep canyon walls may be affected by evanescent modes not accounted for in the model predictions.

In order to examine a possible spatial pattern in model errors, the biases are shown in plan view in Figure 33. The biases reveal that generally the refraction model tends to under predict wave heights at sites onshore of the canyon where the bathymetry causes a divergence of wave energy, while over predicting at the sites where the canyon causes a focusing of wave energy, consistent with the case studies discussed earlier. A positive bias is also noted at sites 26,28,29,30, which lie in the narrow focusing region between the two canyons (see ray diagram Figure 17). In contrast sites 15-17,25,31 on

either side of this focusing region, all display a negative bias. This model tendency may be the result of neglected diffraction effects that tend to disperse wave energy away from regions of focusing and into the sheltered zones. Nevertheless, the extreme variation in wave conditions across the canyons is surprisingly well described by refraction theory.

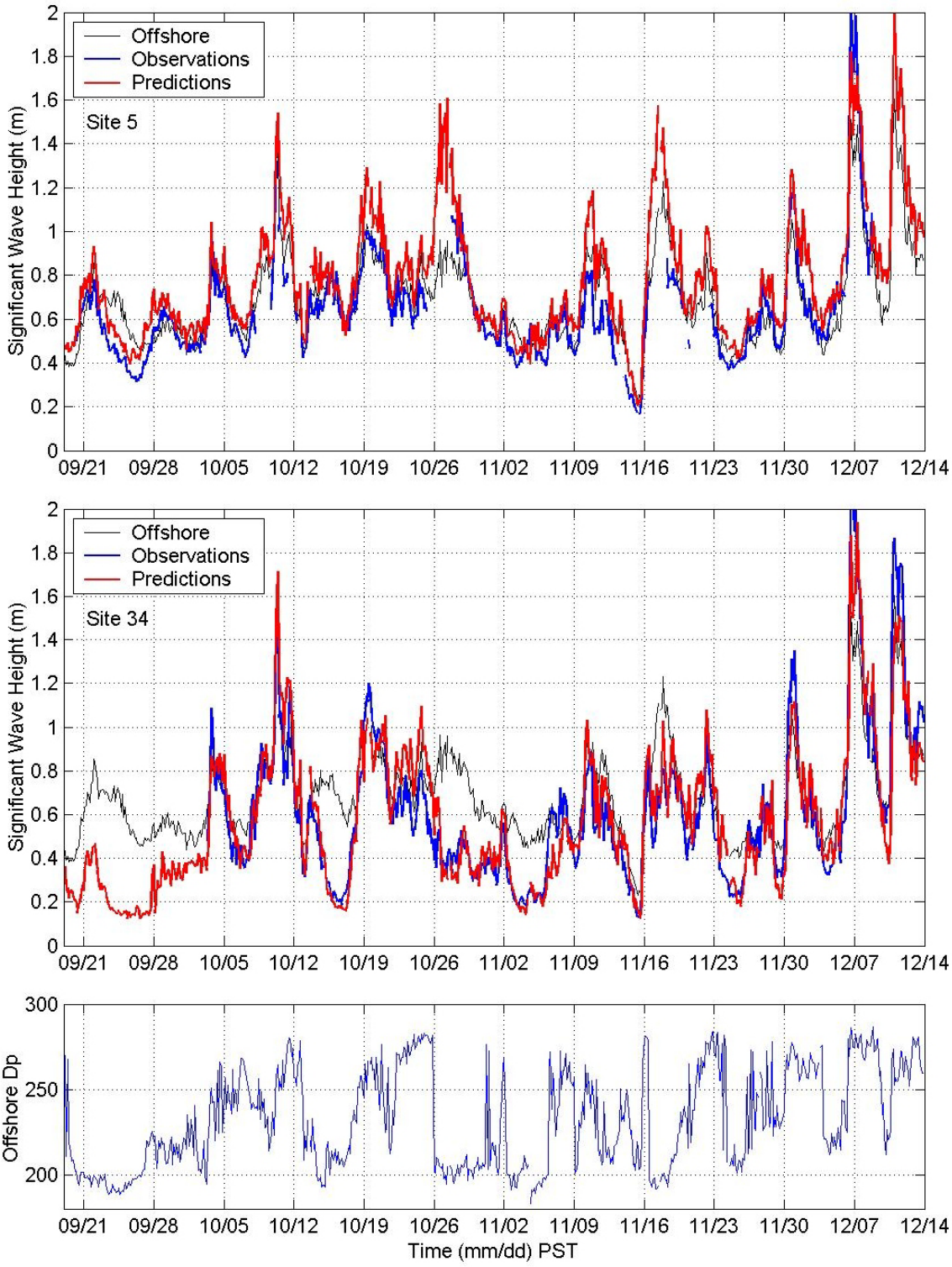

Figure 23. Predicted (red) and observed (blue) significant wave height time series for the duration of the NCEX experiment at the exposed sites 5 and 34. The offshore wave height (the thin line in upper panels) and direction (lower panel) are indicated for reference.

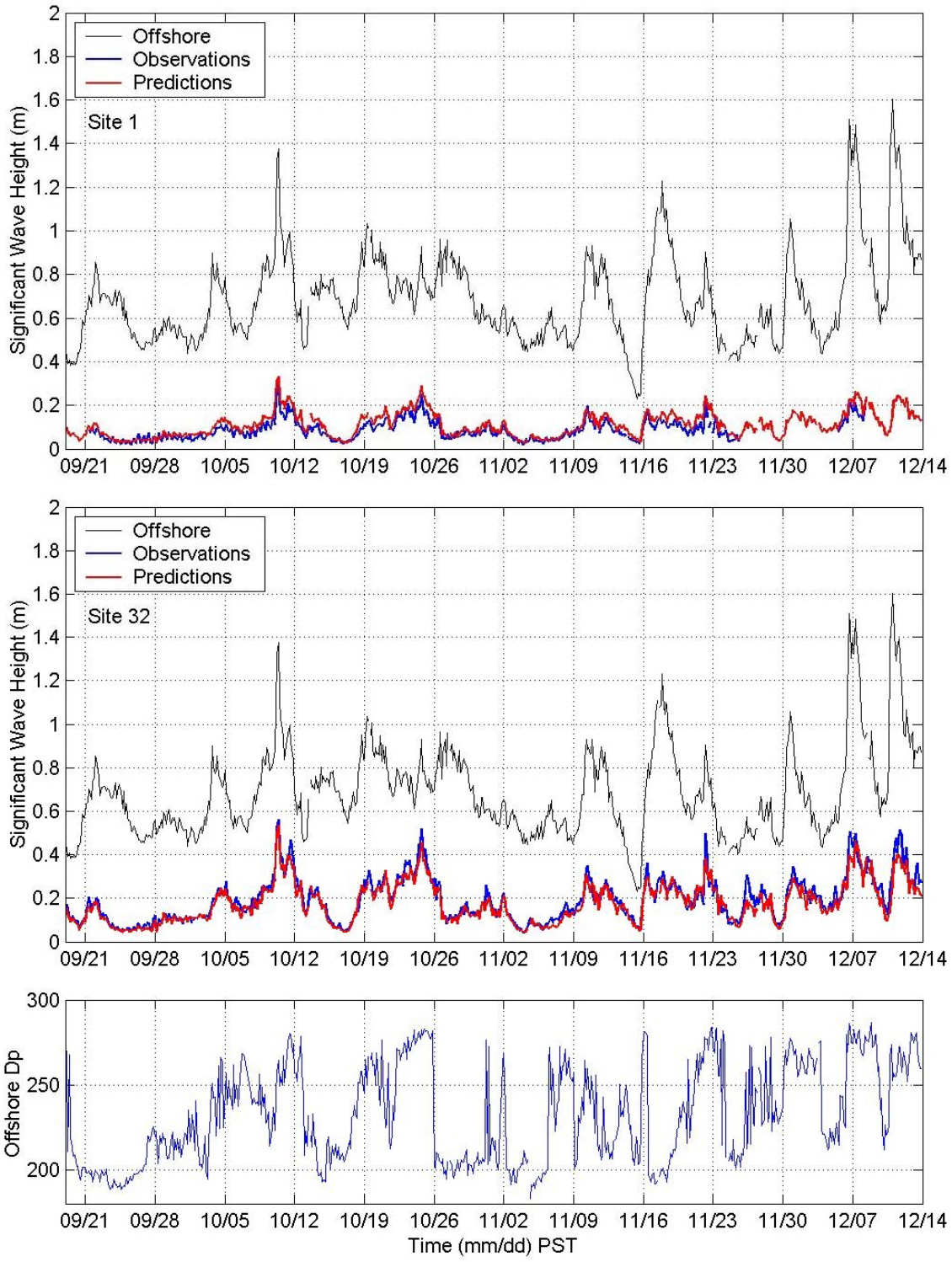

Figure 24. Predicted and observed significant wave height time series for the duration of the NCEX experiment at the sheltered sites 1 and 32. (Same format as Figure 23).

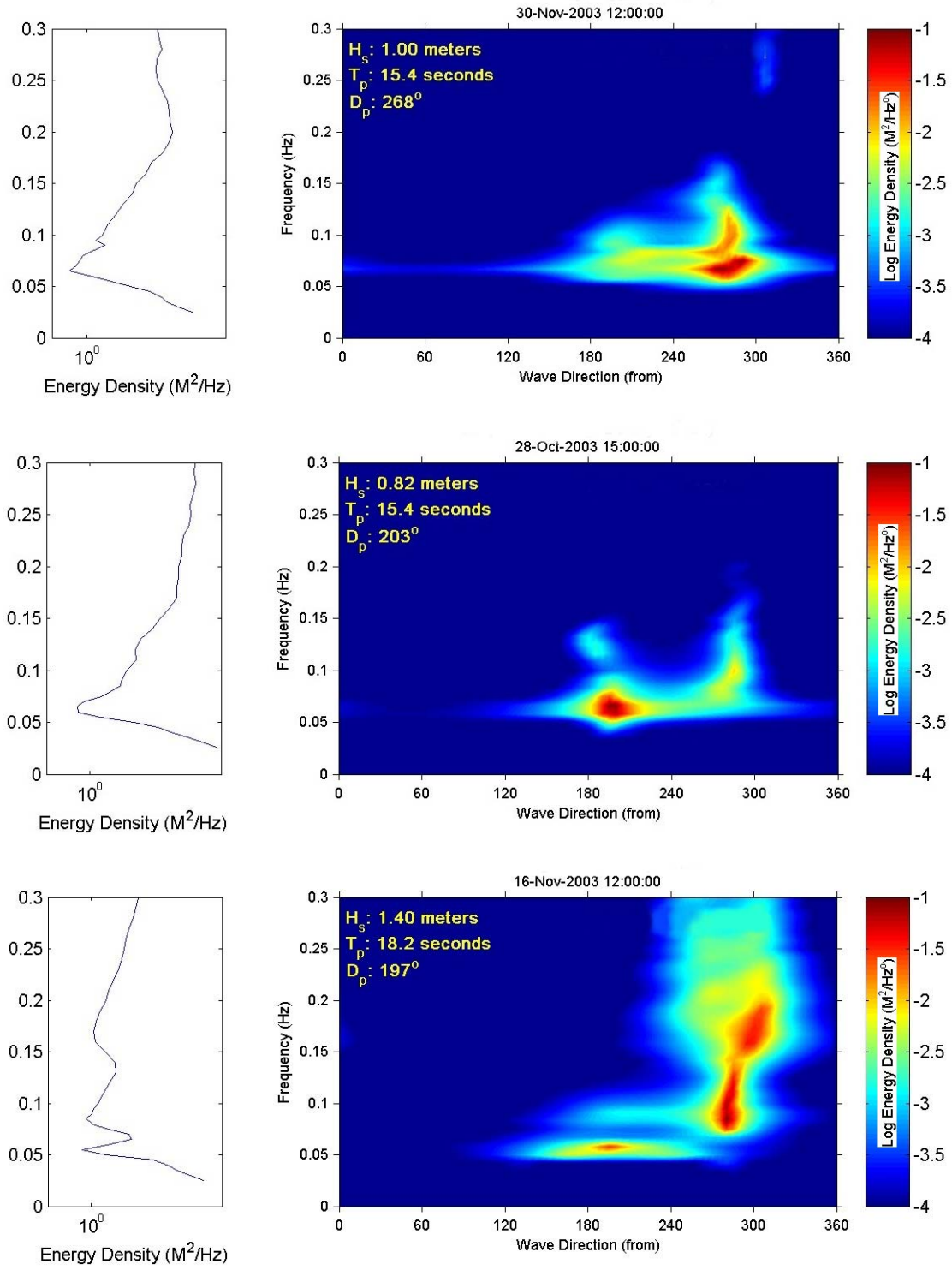

Figure 25. Offshore spectrum for case study I - west swell (top panel), case study II – south swell (middle panel) and case study III – mixed swell (bottom panel). The frequency-directional spectral density $E(f,\theta)$ is indicated in color and the panel on the left shows the frequency spectrum $E(f)$

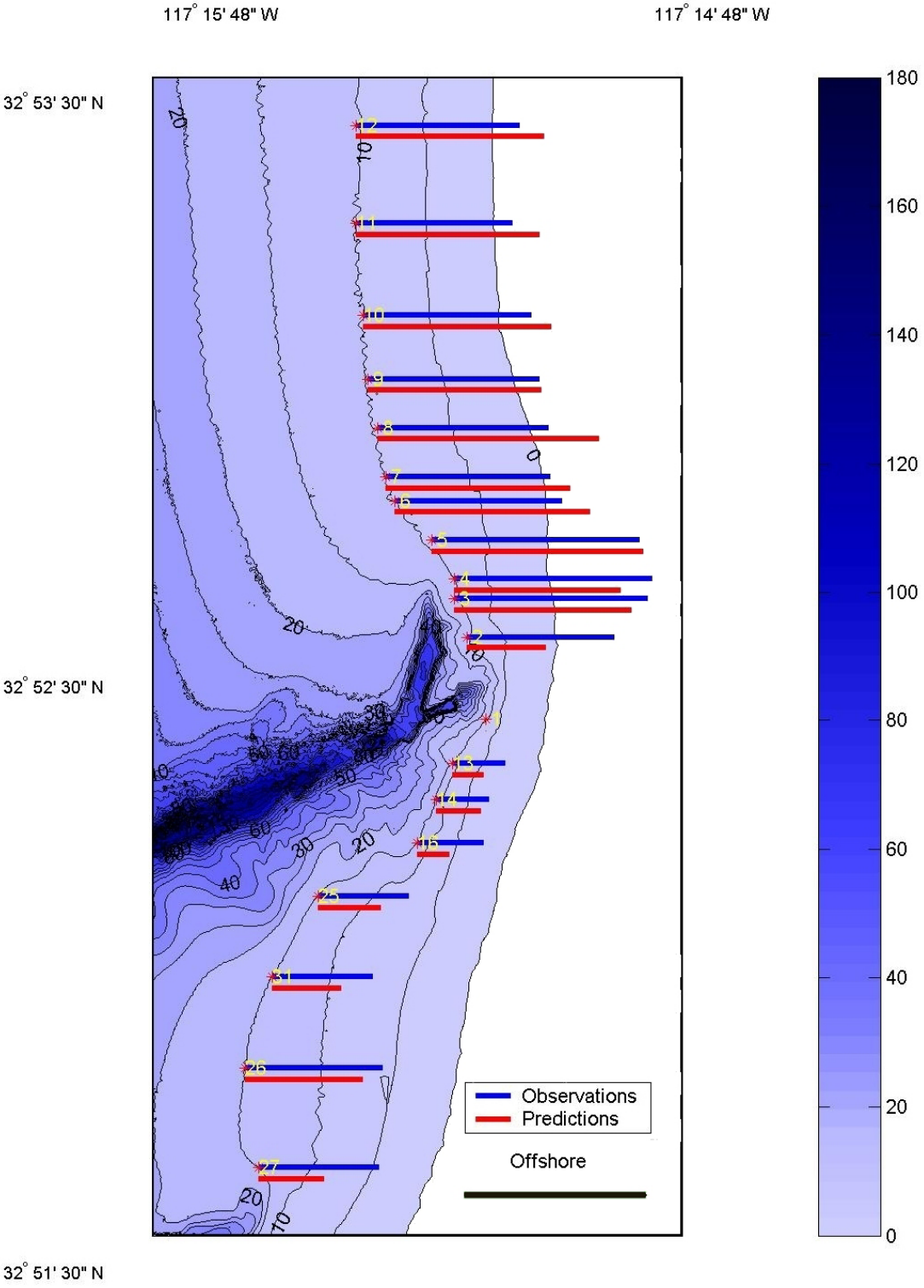

Figure 26. Comparison of observed (blue bars) and predicted (red bars) wave heights for Case I (west swell 1200 PST 30 November 2003). The offshore wave height is indicated for reference with a black bar. Color contours show the underlying bathymetry (units m).

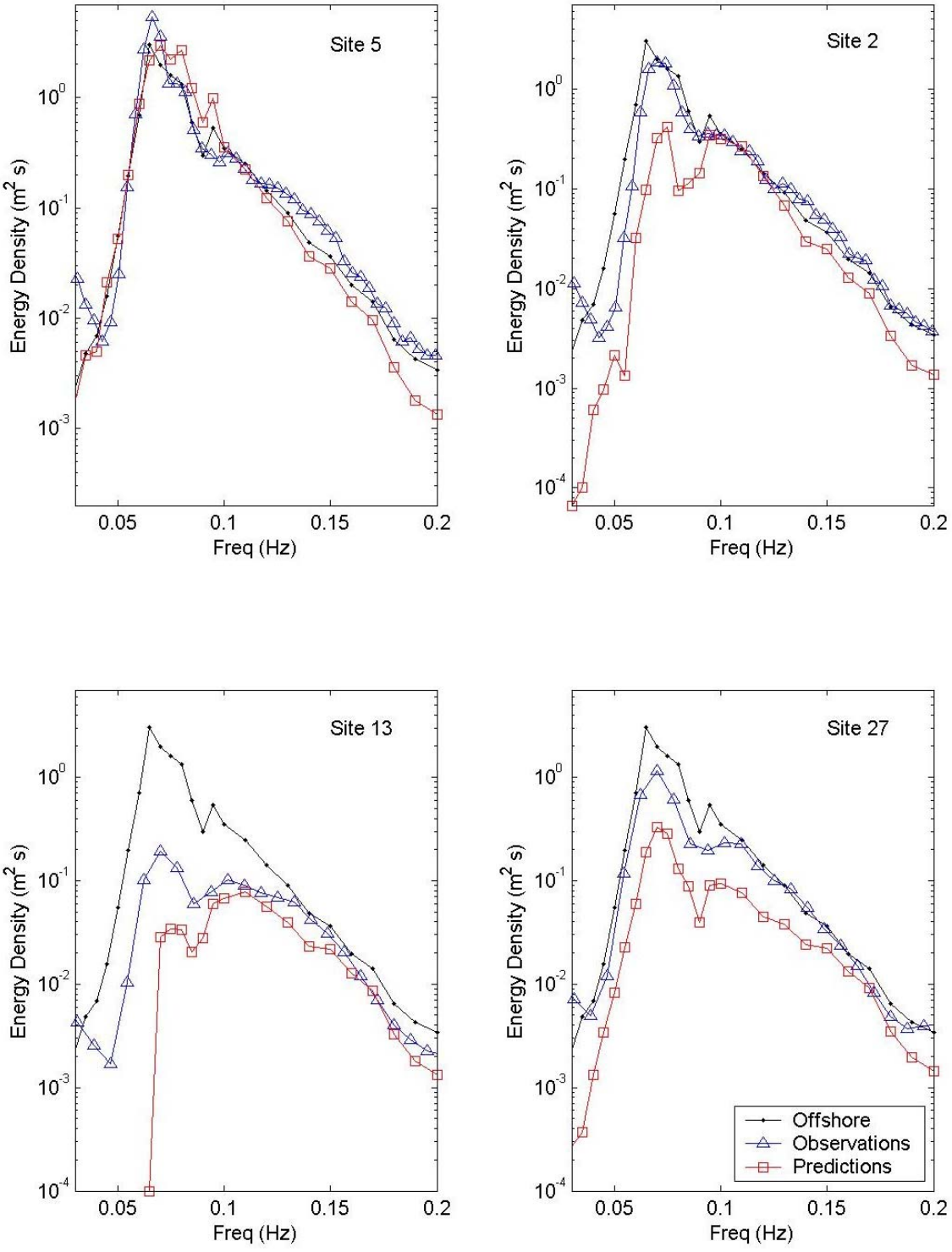

Figure 27. Observed (blue) and predicted (red) energy spectra at four different sites for Case I (west swell 1200 PST 30 November 2003). The offshore spectrum is indicated in each panel with a thin black line.

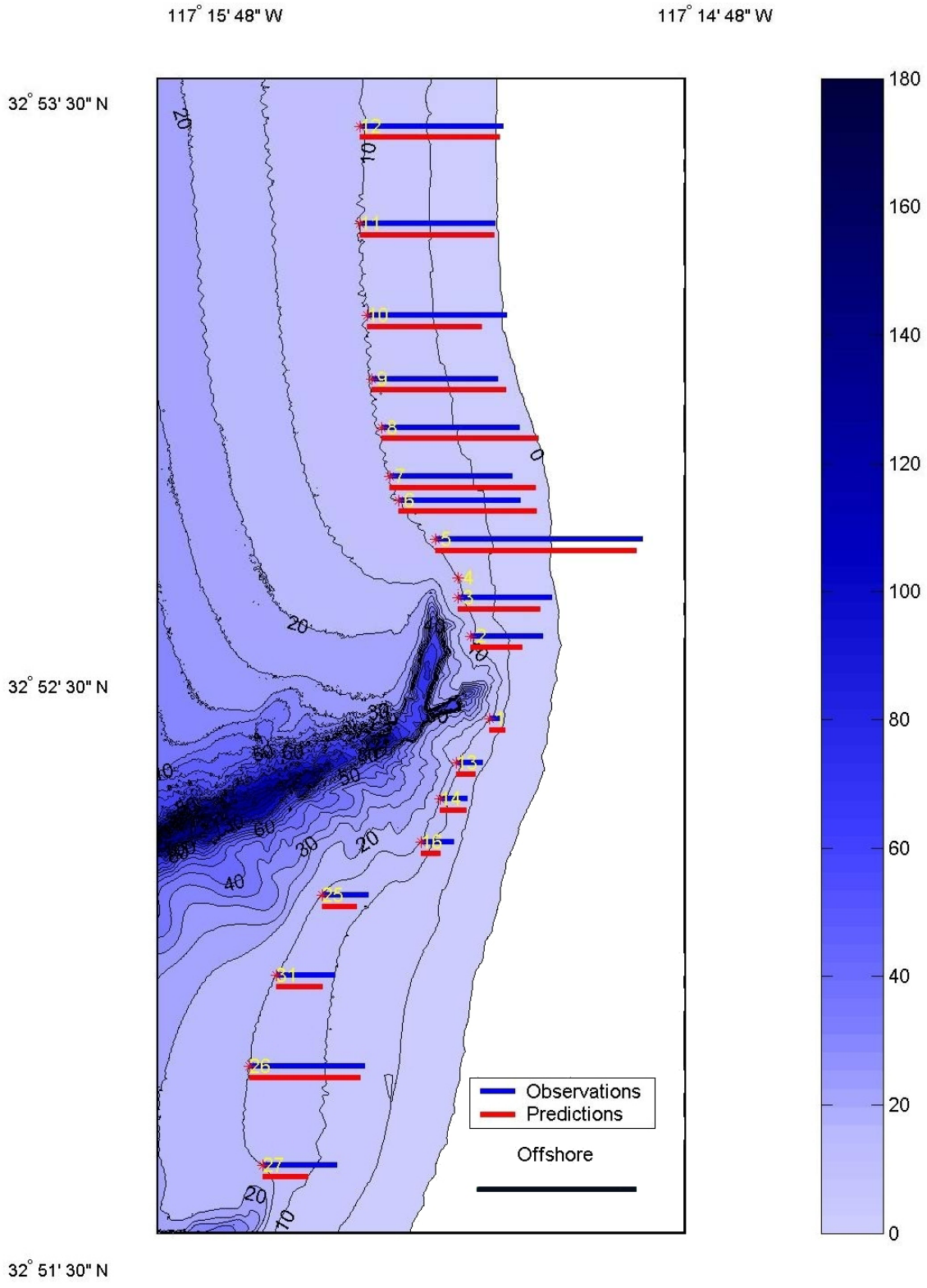

Figure 28. Comparison of observed and predicted wave heights for Case II (south swell 1500 PST 28 October 2003). (Same format as Figure 27).

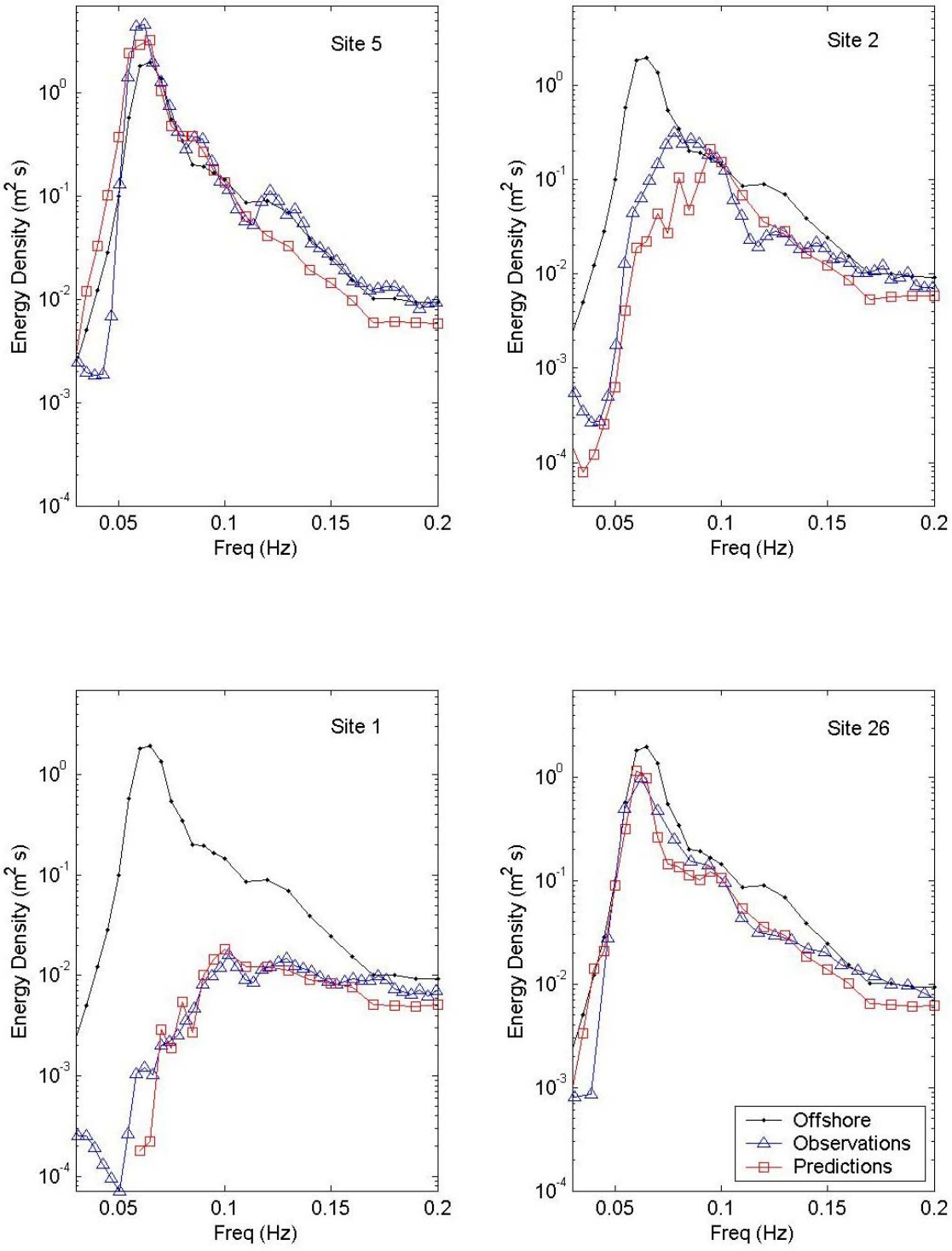

Figure 29. Observed and predicted energy spectra at four different sites for Case II (south swell 1500 PST 28 October 2003). (Same format as Figure 27).

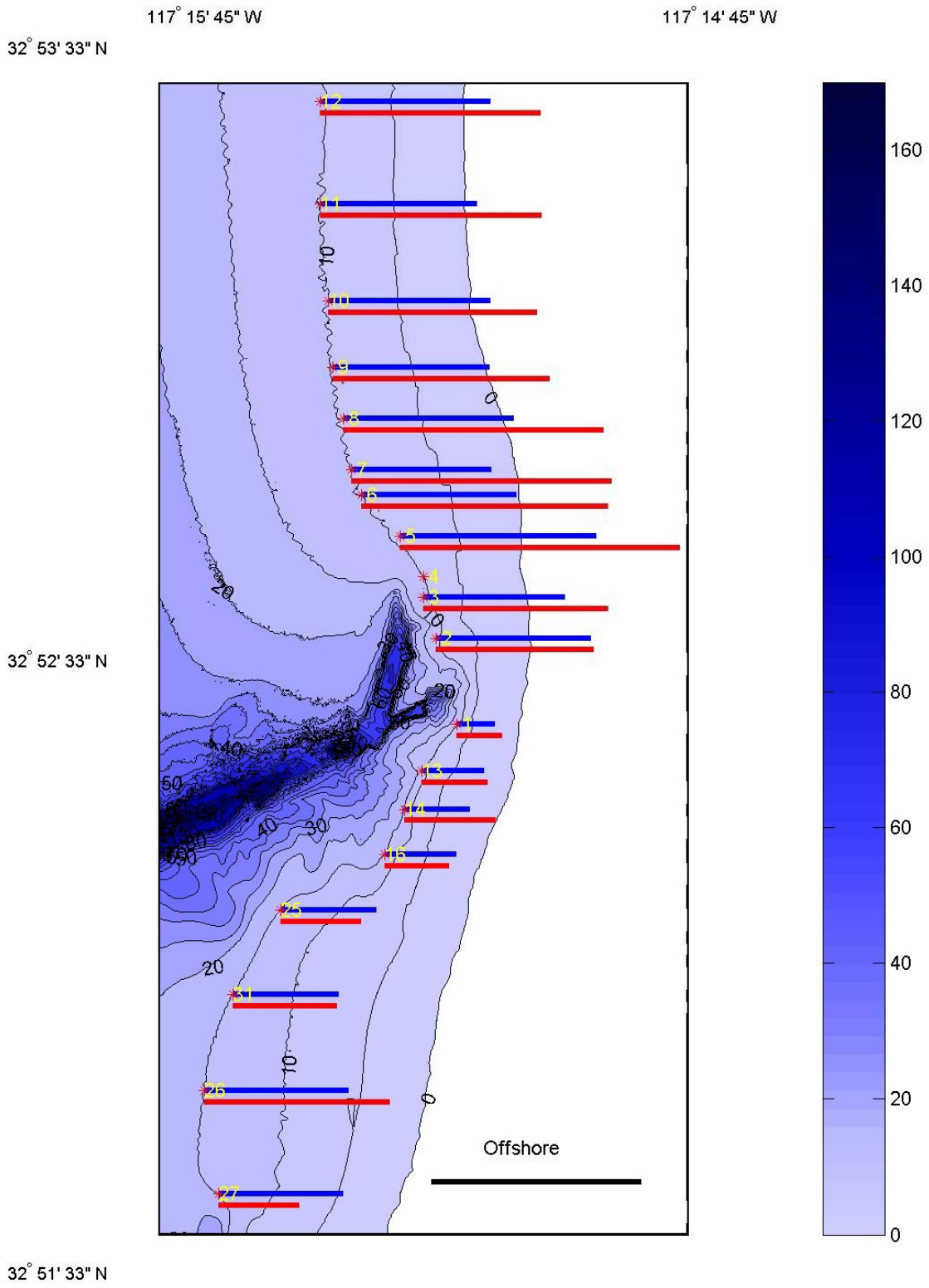

Figure 30. Comparison of observed and predicted wave heights for Case III (mixed swell 1500 PST 16 November 2003). (Same format as Figure 26).

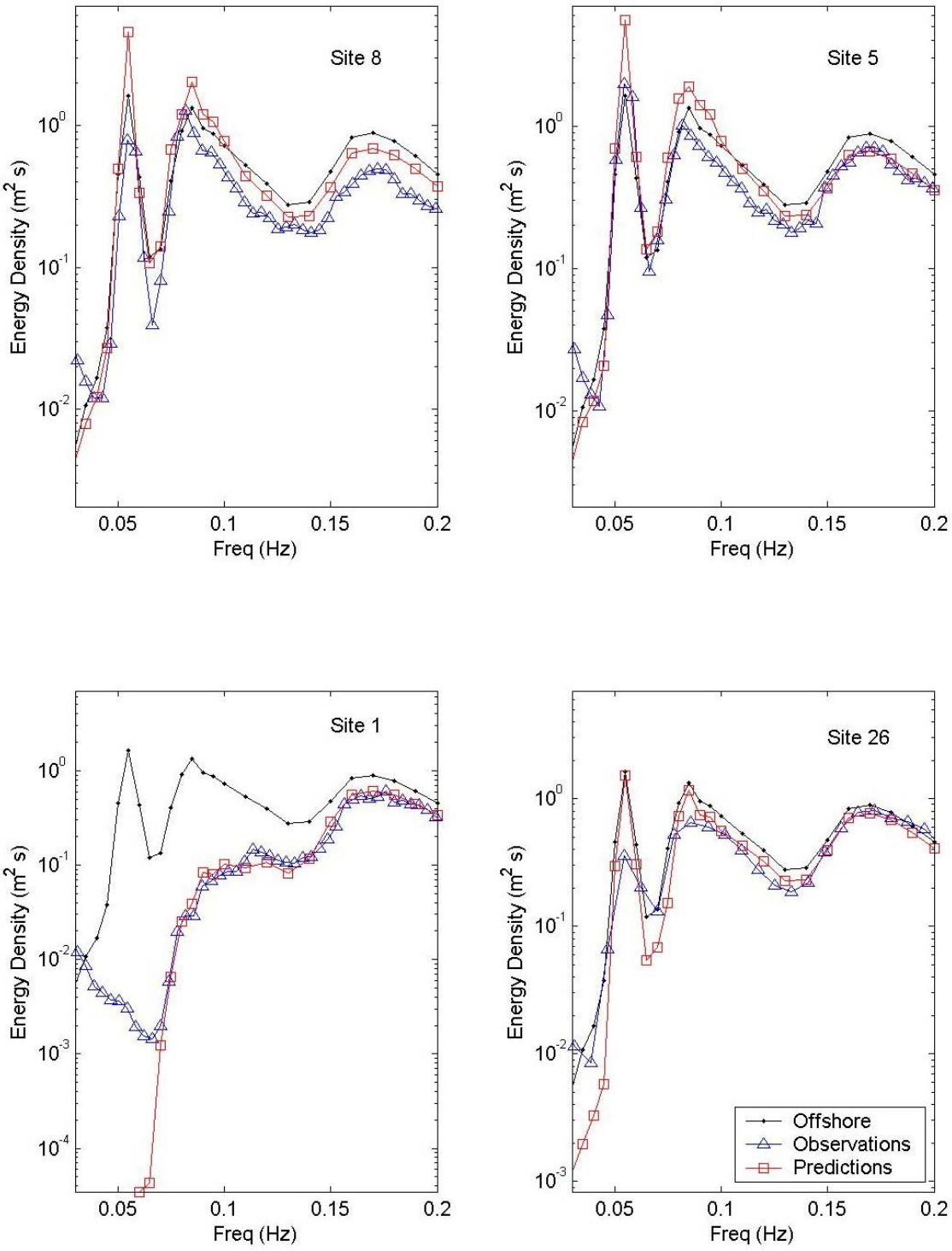

Figure 31. Observed and predicted energy spectra at four different sites for Case III (mixed swell 1200 PST 16 November 2003). (Same format as Figure 27).

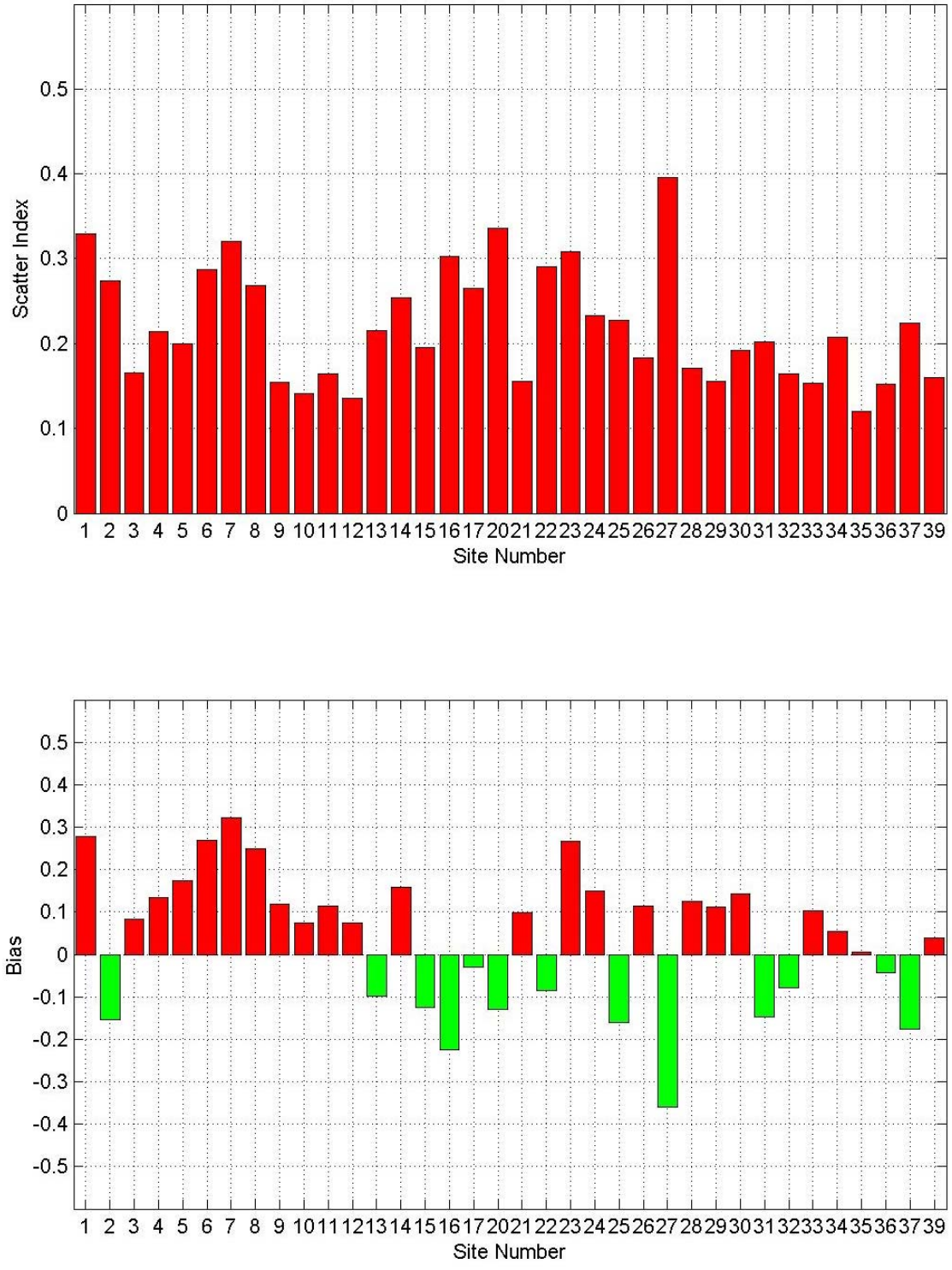

Figure 32. Scatter index (top panel) and bias (bottom panel) of predicted wave height (relative to offshore wave height) at all sites for the entire experiment period. Negative values are indicated in green and positive values in red.

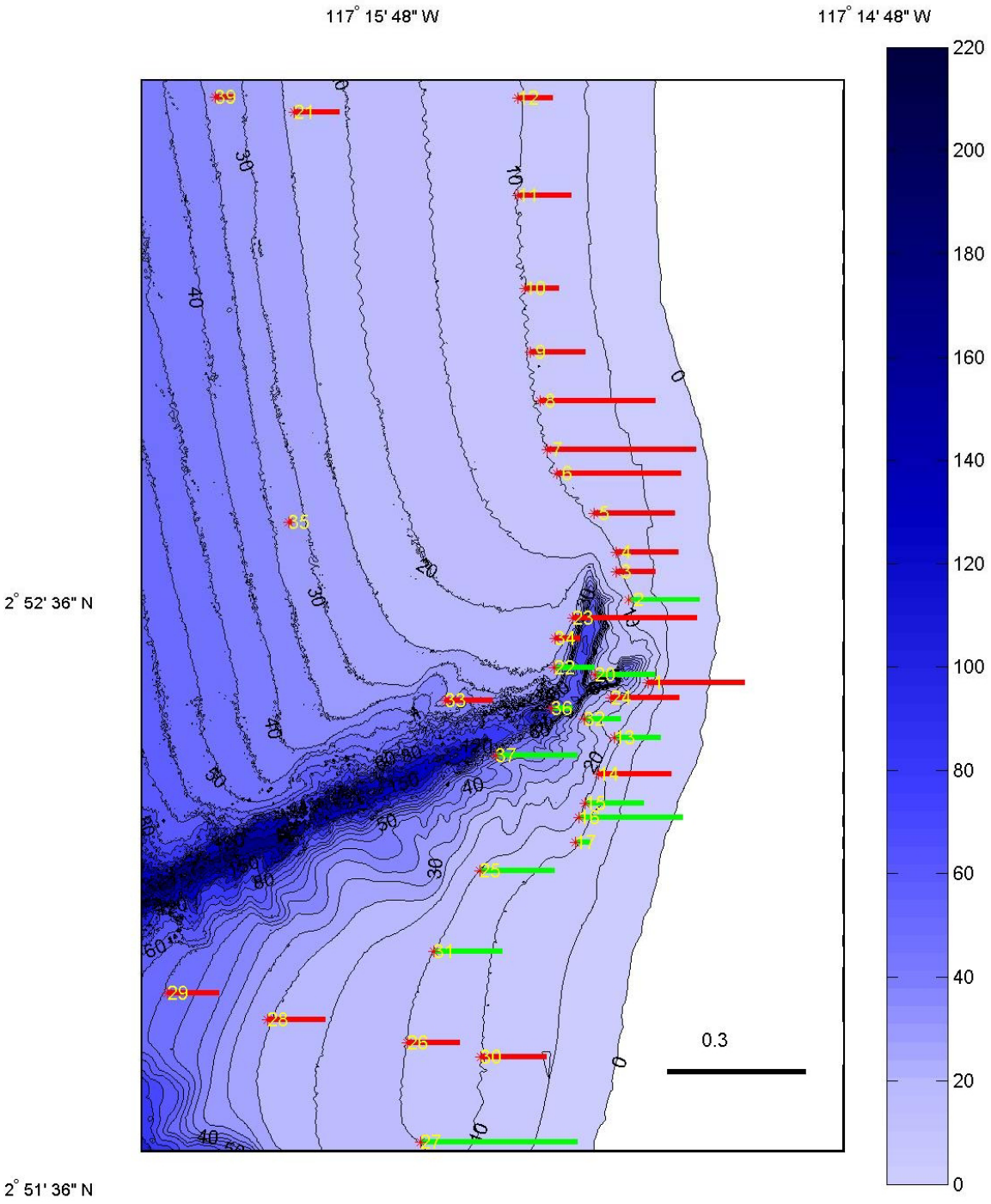

Figure 33. Bias of predicted wave height (relative to offshore wave height) at all sites for the entire experiment period. Negative values are indicated in green and positive values in red. The length of the black scale bar represents a value of 0.3.

VII. SUMMARY AND CONCLUSIONS

The accuracy of linear spectral-refraction theory in areas of complex nearshore bathymetry was examined with 3 months of extensive wave data collected during the Nearshore Canyon Experiment (NCEX) held in the fall of 2003. The field site is characterized by two submarine canyons, La Jolla Canyon and Scripps Canyon, that strongly affect the propagation of long period Pacific swell. Data from 7 directional waverider buoys, 17 bottom pressure recorders, and 12 pressure-velocity sensors, were examined. Analysis revealed large spatial variation in wave energy over the area and extreme variation in the vicinity of the Scripps canyon head, as much as an order of magnitude change in wave height over a few hundred meters. Generally, amplification of swell energy on the north side of the canyon and extremely low energy levels on the south side were observed. In particular, offshore swell arriving from the west was effectively blocked by the canyon. Large variation in both direction and directional spread was also observed. Typically, sites on the seaward side of the canyon featured a large aperture of wave angle arrivals and a broad directional spread, including possible simultaneous swell arrivals from multiple directions and multiple refraction paths. Sites sheltered by the canyon tended to receive a narrow beam of wave energy over a very small aperture of arrival directions.

To examine the role of refraction in the observed extreme wave height variations, orthogonals (rays) were constructed for typical swell arrivals. The refractive effects of the canyons caused a strong divergence of rays away from both canyon heads resulting in strong focusing of rays north of Scripps Canyon head near Black's Beach, and also to a lesser degree between the two canyons. The position and intensification of regions of focusing and divergence was found to have a strong dependence on offshore swell direction and period. Comparisons with directional wave data indicated that the very different swell arrival patterns observed at nearshore sites were consistent with theoretical refraction paths.

Predictions of swell transformation, using a high-resolution spectral back-refraction model were compared to the NCEX observations. To quantitatively assess the

accuracy of the linear refraction model, predictions of standard wave parameters were made for the entire experiment period at each instrument site. The model predictions accurately reproduced the swell arrivals and associated temporal changes in wave heights at most instrument sites over the experiment period. Predictions for three low frequency swell events that are representative of the range of offshore wave conditions were analyzed in more detail. On the whole, the model predicted the observed spatial variation in wave energy with a good degree of accuracy, particularly the large alongshore gradient inshore of the canyons. The model tended to over predict wave heights in regions of wave focusing and under predict wave heights in regions sheltered by the canyons. It was also revealed that when the incident swell peak is particularly narrow, this tendency becomes more pronounced, leading to poorer model results. These errors are believed to be primarily the result of neglected diffraction effects, although close to the steep canyon walls, inaccuracies of the bathymetry grid may also degrade model predictions. The largest error which was observed near the La Jolla canyon head, could be potentially reduced by extending the model domain farther south to satisfy the deep water criteria employed by the model ray calculations.

Overall, the model performance was quite good, with scatter indices (typical errors) of wave height predictions at shallow water sites of about 20 percent. Furthermore, the magnitude of the error tended to decrease the farther away from the canyons that the sites were located. Calculation of the model bias at each site confirmed that the refraction model systematically under predicted wave heights at sites onshore of the canyon where the bathymetry causes a divergence of wave energy, while over predicting at sites where the canyon caused a focusing of wave energy.

In summary, the extreme variation in wave conditions across the canyons is well described by refraction theory, confirming that refraction is the most significant factor in wave transformation in this region. Considering the extreme complexity of the bathymetry and the long period swell, the agreement of observations and model predictions is surprisingly good. Thus, the use of high-resolution spectral-refraction models to forecast waves in areas of complex nearshore bathymetry shows great promise for operational applications.

LIST OF REFERENCES

Athanassoulis, G.A. and Belibassakis, K.A., "A consistent coupled-mode theory for the propagation of small-amplitude water waves over variable bathymetry regions," *J. Fluid Mech*. v. 389, pp. 275-301, 1999.

Berkoff, J. C. W., "Computations of combined refraction-diffraction," *Proc. 13th Coastal Engineering Conference 20*, pp.1249-1263, 1972.

Booij, N., "A note on the accuracy of the mild-slope equation," *Coastal Engng*, v. 7, pp. 191-203, 1983.

Booij, N., Ris, R.C. and Holthuijsen, L.H., "A third-generation wave model for coastal regions. 1. Model description and validation," *Journal of Geophysical Research*, v. 104(C4), pp. 7649-7666, 1999.

Dalrymple, R.A., "Model for refraction of water waves," *J. Waterway. Port. Coastal Ocean Eng*., v. 114, no.4, pp. 423-435, 1988.

Dobson, R. S., "Some applications of a digital computer to hydraulic engineering problems," *Tech. Rep. 80*, Department of Civil Engineering, Stanford University, 185 pp, 1967.

Emery, K.O., "Wave patterns off Southern California, *Journal of Marine Research*, v.17, pp.133-140, 1958.

Herbers, T.H.C., Hendrickson, E.J. and O'Reilly, W.C., "Propagation of swell across a wide continental shelf," *J. Geophysical Research*, v.105(C8), pp.19729-19737, 2000.

Herbers, T.H.C., Elgar S., and Guza, R.T., "Directional spreading of waves in the nearshore," *J. Geophys. Res.*, v.104(C4), pp.7683-7693, 1999.

Kinsman, B., *Wind Waves: Their generation and propagation on the ocean surface*, Prentice Hall, New Jersey, 1964.

Kirby, J.T. and Dalrymple, R.A., "Verification of a parabolic equation for propagation of weakly non-linear waves," *Coastal Engineering*, v.8, pp. 219-232, 1984.

Kirby, J.T., and Dalrymple, R.A., "Modeling waves in surfzones and around islands," *J Waterway. Port. Coastal Ocean Eng.*, v.112, no.1, pp.78-93, 1986.

Kirby, J.T., "Higher-order approximations in the parabolic equation method for water waves," *Journal of Geophysical research*, v. 91(C1), pp.933-952, 1986.

Kirby, J. T. and Dalrymple, R. A., "Combined Refraction/Diffraction Model REF/DIF 1, Version 2.5. Documentation and User's Manual", *Research Report No. CACR-94-22*, Center for Applied Coastal Research, Department of Civil Engineering, University of Delaware, Newark, 1994.

Komar, P.D., *Beach Processes and Sedimentation*, Prentice Hall Inc., New Jersey, 1998.

Komen, G.J., Cavaleri, L., Donelan, M., Hasselmann, K., Hasselmann, S., and Janssen, P.A.E.M., *Dynamics and Modelling of Ocean Waves*. Cambridge University Press, 1994.

Kuik, A.J., Van Vledder, G.P., and Holthuijsen, "A method for the routine analysis of pitch-and-roll buoy wave data," *J. Phys. Oceanogr.,* v.18, pp.1020-1034, 1988.

Long, R.B., "The statistical evaluation of directional spectrum estimates derived from pitch/roll buoy data," *J. Phys. Oceanogr*., v. 10, pp.944-952, 1980.

Longuet-Higgins, M.S., "On the transformation of a continuous spectrum by refraction," *Proc. Cambridge Philos. Soc*., v.53, pp.226-229, 1957.

Longuet-Higgins, M.S., Cartwright, D.E. and Smith, N.D., "Observations of the directional spectrum of sea waves using the motions of a floating buoy," *In Ocean Wave Spectra, proceedings of a conference,* Easton, Maryland, pp. 111-136. National Academy of Sciences, Prentice-Hall, 1963.

Lygre, A., and H. E. Krogstad, "Maximum entropy estimation of directional distribution in ocean wave spectra," *J. Phys. Oceanogr.,* v.16, pp.2052-2060, 1986.

Massel, S., "Extended refraction-diffraction equations for surface waves," *Coastal Engineering*, v.19, pp. 97-126, 1993.

Massel, S., *Ocean surface waves: their physics and prediction. Advanced series on ocean engineering. volume.11*, World Scientific. Singapore, 1996.

Munk, W.H., and Arthur, R.S., "Wave intensity along a refracted ray," in *Gravity Waves, Circ. 521*, pp. 95-108, Natl. Bur. of Stand. 1952.

Munk, W.H., and Traylor, M.A., "Refraction of ocean waves: a process linking underwater topography to beach erosion," *J. Geol.*, v.55, no.1, pp.1-26, 1947.

Munk, W.H., Miller, G.R., Snodgrass, F.E., and Barber, N.F., "Directional recording of swell from distant storms," *Phil. Trans. Roy. Soc. Lon.*, A255, pp.506-584, 1963.

O'Reilly, W.C., and Guza, R.T., "Comparison of spectral refraction and refraction-diffraction wave model," *J. Waterway. Port. Coastal Ocean Eng*., v.117. no.3 pp.199-214, 1991.

O'Reilly, W.C., and Guza, R.T., "A comparison of two spectral wave models in the Southern California Bight," *Coastal Engineering*, v. 19, pp.263-282, 1993.

O'Reilly, W.C., "The Southern California wave climate: effects of islands and bathymetry," *Shore and Beach*, v. 61, no. 3, pp.14-19, 1993.

Pawka, S.S., "Island shadows in wave directional spectra," *Journal of Geophysical Research,* 88(C4), pp.2579-2591, 1983.

Pawka, S.S., Inman, D.L., and Guza, R.T., "Island sheltering of surface gravity waves: model and experiment," *Continental Shelf Research*, v.3, no.1, pp.35-53, 1984.

Pierson, J.P., Neumann, G., and James, R.W., *Practical Methods for observing and forecasting ocean waves by means of wave spectra and statistics*, U.S. Naval Oceanographic Office, H.). Pub No. 603, 1955.

Porter, D., and Staziker, D.J., "Extensions of the mild slope equation," *J. Fluid Mech.*, v.300, pp.367-382, 1995.

Radder, A.C., "On the parabolic equation method for water-wave propagation," *Journal of Fluid Mechanics*, v.95, part 1, pp.159-176, 1979.

Ray, T. A., *Wave propagation over complex bathymetry*, Master's Thesis, Naval Postgraduate School, Monterey, California, June 2003.

Shepard, F.P., and Inman, D.L., "Nearshore water circulation related to bottom topography and wave refraction," *Transactions*, American Geophysical Union, vol.31, no.2, p.196-212, 1950.

Snodgrass, F.E., Groves, G.W., Hasselmann, K.F., Miller, G.R., Munk, W.H., and Powers, W.H., "Propagation of ocean swell across the Pacific," *Phil. Trans.Roy. Soc. Lon*., v.259, pp.431-497, 1966.

Tolman, H.L., "User Manual and System Documentation of WAVEWATCH-III version 1.18", *NCEP Technical Note*, National Center for Environmental Prediction. 110pp, 1998.

U.S. Army Coastal Engineering Research Center (CERC), *Shore Protection Manual Volume 1*.Books for Business, New York, 2001.

INITIAL DISTRIBUTION LIST

1. Defense Technical Information Center
   Ft. Belvoir, Virginia

2. Dudley Knox Library
   Naval Postgraduate School
   Monterey, California

3. Professor T.H.C. Herbers, Department of Oceanography (Code OC/He)
   Naval Postgraduate School
   Monterey, California

4. Professor E.B. Thornton, Department of Oceanography (Code OC/Tm)
   Naval Postgraduate School
   Monterey, California

5. Mr Paul Jessen, Department of Oceanography
   Naval Postgraduate School
   Monterey, California

6. CMDR Andrew McCrindell
   Directorate of Oceanography and Meteorology
   Sydney, NSW, Australia

7. LEUT Scott Peak
   Directorate of Oceanography and Meteorology
   Sydney, NSW, Australia